# Complex zoning in clinopyroxenes from Marion Island

Andries Eliza Johannes Botha

DEPARTMENT OF GEOLOGY
FACULTY OF NATURAL AND AGRICULTURAL SCIENCES
**UNIVERSITY OF PRETORIA**

# DECLARATION OF ORIGINALITY

# UNIVERSITY OF PRETORIA

Full names of student: **Andries Eliza Johannes Botha**

Topic of work: **Complex zoning in clinopyroxenes from Marion Island**

**Declaration**

1. I understand what plagiarism is and am aware of the University's policy in this regard.

2. I declare that this thesis is my own original work. Where other people's work has been used (either from a printed source, Internet or any other source), this has been properly acknowledged and referenced in accordance with departmental requirements.

3. I have not used work previously produced by another student or any other person to hand in as my own.

4. I have not allowed, and will not allow, anyone to copy my work with the intention of passing it off as his or her own work.

**SIGNATURE**

…….
A.E.J Botha

# Acknowledgement

First and foremost I would like to acknowledge the help and support I received from my principal supervisor, Dr. R.J. Roberts. I would also like to acknowledge the help and support from my late co-supervisor Mr. Peter Gräser, with analytical methods, equipment (specifically the microprobe) and in coordination with the Cameca factory in Paris, France; the Cameca factory in Paris, France for their time and help; the Microanalysis lab at the University of Pretoria, for their help and time on their equipment and access to their labs, especially Miss Antoinette Buys and Mr A.J. Botha for discussions on SEM and EDS analysis; the South African National Antarctic Program (SANAP) and Prof. A.J. Bumby for the opportunity to be part of the 2009 take over expedition, where samples were collected. For intellectually stimulating conversations and discussion I would like to thank the Geology department of the University of Pretoria.

# Abstract

Euhedral clinopyroxene mega-crystals have been retrieved from Marion Island, a volcanic island situated on an inactive transform fault near the mid oceanic ridge on Antarctic tectonic plate and part of the Prince Edward Island group. The island is considered to be the product of hotspot- related volcanism. Clinopyroxene megacrysts were sampled from the southern side of the island on a scoria cone named Pyroxene Hill. Several analytical methods including Energy Dispersive Spectrometry (EDS), Electron Probe Microanalysis (EPMA) and EPMA-mapping were utilized in investigating the zoning found within these 5-10 cm large crystals. The zoning found was “patchy”, in that it did not conform to commonly described zoning such as normal, reverse, sector or oscillatory, but rather consisted of chemically distinct areas with either diffuse or sharp boundaries, not orientated parallel to the grain boundaries or crystal lattice. The chemistry of the crystals indicates that they have formed from an evolved basaltic melt, and are likely to have crystallised at a depth of 15- 30 km.

A model is postulated for the formation of these crystals in which the megacrysts crystallise rapidly from a supersaturated melt. Pre-existing crystalline material undergoes imperfect diffusion at high temperature to create a patchwork of compositional zones. Supersaturation likely requires a volatile-rich melt, which undergoes rapid degassing owing to an external trigger. The presence of a transform fault directly below Marion Island may provide a seismic trigger for such a degassing event.

# Contents

# List of tables

# List of figures

# Chapter 1: Introduction

## *1.1 Introduction*

The main extrusive products of volcanism are the lavas and pyroclastic deposits produced during eruption. The textures preserved in these deposits, the stratigraphy of the different deposits, and the chemistry of the deposits can all be used to investigate the processes which lead to the eruption. In many cases, these deposits indicate a complex magmatic history in which multiple eruptive episodes are linked to an evolving magma chamber. In particular, crystals present in the deposits may record complex magmatic history in the form of zoning and chemical changes.

Marion Island in the sub-Antarctic Indian Ocean is a relatively under-studied volcanic island made up of the products of numerous eruptive events. Amongst the different volcanic layers are numerous scoria cones, which commonly contain of numerous very large clinopyroxene crystals. Though sampling access to the island is restricted by the South African government, samples of these clinopyroxene crystals, measuring 1- 5 cm in diameter, have been obtained, and are the focus of this study.

These large crystals could provide insight into the record of the magmatic history of the island and more specifically the scoria cone from which it came, in the form of chemical variations in zones and domains within the crystals, which may reflect a residence history in the magma chamber, which can be measured through a variety of electron beam techniques. Analytical methods such as Scanning Electron Microscope (SEM) Energy Dispersive Spectrometry (EDS), backscatter imagery and Electron Probe Microanalysis (EPMA) have been used to identify and investigate the clinopyroxene crystal chemistry. This dissertation presents the results of these investigations, and then discusses the implications of the chemical variation and zoning identified in the crystals.

*1.2 Regional geology of Marion Island*

Marion Island is the younger sister of two volcanic islands known as the Prince Edward Island Group. Situated in the sub-Antarctic Indian Ocean, Marion Island (46°54'S, 37°45'E) lies approximately 2° north of the Antarctic polar front (Fig. 1), and about 2130 km south-east of the southernmost tip of Africa and 2570 km north of Antarctica. Marion Island forms the top part of an oval shaped multiplate shield volcano, which is lying on a small oceanic plateau (Sumner, 2004; Chevalier 1986). The island's subaeriel extent measures 290 $km^2$, with the highest peak, Mascarin Peak, at 1240 m above sea level (Fig. 3; Sumner, 2004)..

Marion Island is situated on the Antarctic plate, 250 km south east of the South West Indian mid-oceanic ridge, striking 070° (based on maps by Royer *et al.,* 1989 & Google Earth imagery, 2009) (Fig. 2). According to Royer *et al.* (1989) the main spreading rate of the South West Indian Mid Oceanic Ridge is about 1 $cm.a^{-1}$. The island is also situated directly on the inactive remnants of a transform fault neighbouring and parallel to the Prince Edward transform fault to the east (Fig. 2).

Marion and Prince Edward Islands form the top peaks of an extensive oval shaped shield volcano that strikes in accord with the transform fault running through the middle of the shield (Fig. 2), striking 15°-20°. Whether the two islands are of the same shield or two inter-grown shields is not clear in the literature (very little reference is made to the volcanic shields). The overall shape of Marion Island itself shows obliqueness in the east-west direction, which is perpendicular to the Prince Edward Fracture zone (Chevallier, 1986).

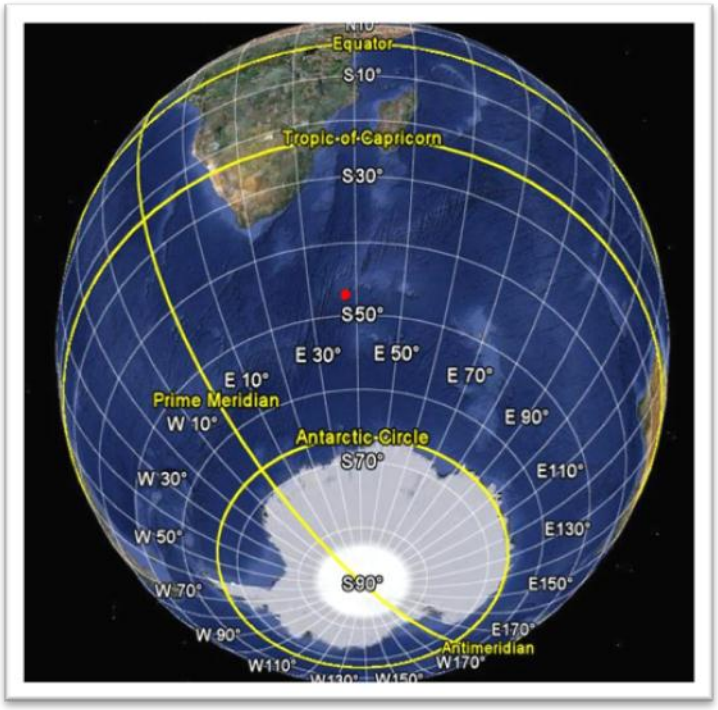


**Figure 1: The red dot marks the location of the Prince Edward Islands at 46°54'S, 37°45'E (Google Earth, 2009)**

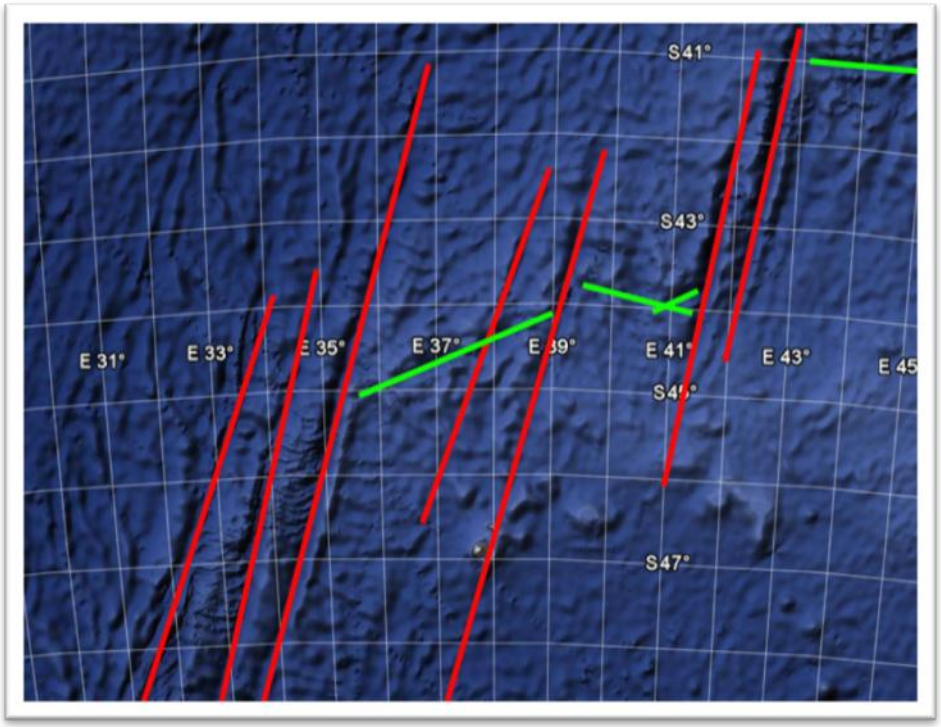


**Figure 2: Image showing the strike lines of the South Western Indian Mid Oceanic Ridge (in green) and the transform faults (in red) (Google Earth, 2009).**

According to McDougall *et al.* (2001), Marion Island, together with the nearby Funk Seamount and neighbouring Prince Edward Island, indicates the position of a “long lived” hotspot. It is further suggested by McDougall *et al.* (2001) that the Marion hot-spot can be backtracked over the past 100 Ma, as the African plate moved in a northern direction over the hotspot. The postulated hot spot track forms a J-shaped track through Volcan de l’ Androy in South-eastern Madagascar (which is believed to mark the focal point of the plume at 88 Ma), to the east coast of Madagascar (McDougall *et al.,* 2001). Furthermore it is suggested by McDougall *et al.* (2001), that at the time when the plume was located at Volcan de l’Androy (at 88 Ma), it played an active role in the separation of greater India from Madagascar.

### *1.3 Geology of Marion Island*

The surface topography of the island is dominated by scoria cones, pyroclastic flow deposits, younger black lava flows (such as pahoehoe and aa flow types), to a lesser extent the much older grey lavas and a large remnant of a massive landslide (Chavallier, 1987) on the southern side (Fig. 3). Marion Island is regarded as being an active volcano, as the last major eruption occurred in 1980, when a 9 km long en-echelon fissure, stretching from the coast to the summit, opened up on the western side of the island (Le Masurier et al., 1990). Le Masurier *et al*. (1990) calculated that 5 000 000 $m^3$ of lava erupted out of this fissure.

No active seismic surveys have been conducted on the island, owing to the massive influence wave action on the coastline of the island has on seismic readings. The only geological investigations (Chevallier, 1986; Verwoerd, 1971; Verwoerd *et al.,* 1987; McDougall, 2001; le Roux, 2012) that have been done on the islands have been reliant on outcrops, outcrop sampling and remote sensing data. No core or exploration drilling has been done on the island.

Marion Island is geologically a young island (<0.45 Ma) of which the geology can be classed into three main units (Fig. 3): the older grey lava unit, the younger black lava unit and the successions of scoria (Verwoerd, 1971 in McDougal *et al.,* 2001; LeMasurier *et al.,* 1990). The older grey lava unit is between 450 ka and 100 ka in age, while the younger black lava unit date from ±11 ka to the present with the last eruption in 1980. The scoria is present throughout the grey and black lava unit's history (McDougal *et al*., 2001).

The older grey lava unit consist of alkaline basalt lava flows which are interbedded with pyroclastics from two volcanic periods and intercalated tills, and these tills are found at the beginning and the end of each of the volcanic periods (Boelhouwers *et al*., 2008). The black lava consists of three types of lava flows; aa, pahoehoe and block lava (Boelhouwers *et al.,* 2008 & McDougall *et al.,* 2001). The third unit, scoria, is present in between successive black and grey lava flows. Currently over 130 scoria cones can be found scattered in a semi radial pattern on the island (Boelhouwers *et al.,* 2008 & McDougall *et al.,* 2001).

Petrologically the black and grey lavas belong to the alkaline oceanic island basalts (OIB), $SiO_2$ values between 45–48 wt % with three sample reporting $SiO_2$ values of 50, 56 and 69 wt % respectively (McDougall *et al*., 2001; le Roex *et al.,* 2012). Analysis of the lead (Pb) and strontium (Sr) isotope ratios indicate that the lavas found at Marion Island are derived from a mantle source. Furthermore, comparing the Sr isotope data from Prince Edward Island to that of Marion Island shows that the two neighbouring islands were not derived from the same source (McDougall et al, 2001; Verwoerd, 1990 in McDougall *et al*., 2001).

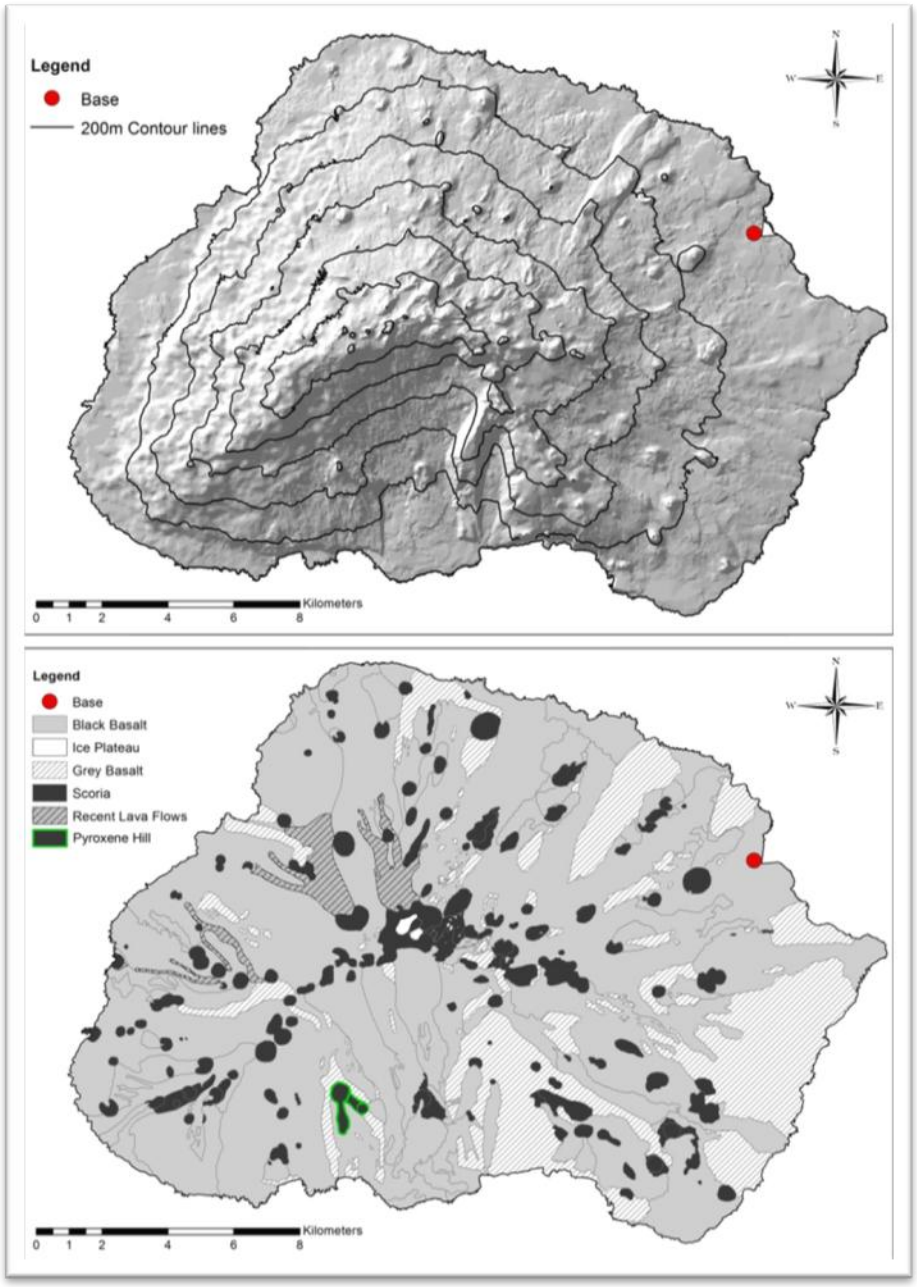


**Figure 3: Topographic hill shade image of Marion Island and simplified geological map of Marion Island (modified after Verwoerd, 1971; Chevallier, 1986; McDougal *et al*., 2001)**

The oldest age obtained for the lavas on Marion Island is 450 ka; furthermore it is indicated by McDougall *et al.* (2001) that the sub-aerial lava flows of Marion and Prince Edward Island are younger than a million years in age. McDougall *et al.* (2001) also suggested through means of K-Ar dating techniques, on whole rock fusion beads, that the volcanic activity of Marion Island was episodic

(McDougall *et al*., 2001). Using this dating method McDougall *et al. (*2001) identified eight definitive volcanic episodes:

Stage I – 450-420 ka,
Stage II – 350 ka,
Stage III – 240 ka,
Stage IV – 170 ka,
Stage V – 110 ka,
Stage VI – 85 ka,
Stage VII – 50 ka,
Stage VIII - <10 ka

Chevallier (1986) suggested that the Marion volcano is composed of two coalescent volcanic shields with separate respective centres of eruption; however these are not easily distinguishable on morphological grounds. This suggestion was based on analysis of the “two sets of radial fractures along which all of the lateral Holocene strombolian eruptions took place” (Chevallier, 1986), allowing a division into a smaller western and a main eastern shield distinction.

According to LeMasurier *et al.* (1990) and le Roex *et al.* (2012) whole rock analysis of Marion Samples resulted in a distribution of basalts, hawaiites, mugearite, benmoreite, and one anomalous rhyolite (Fig. 4). The rhyolite is described as a xenolith within the lava (le Roex *et al.,* 2012). LeMasurier *et al.* (1990) further classified the basalts and hawaiites into four different types on basis of textural grounds which they believed had “clearly evolutionary significance”.

The LeMasurier *et al.* (1990) classification types I and II are believed to have erupted from both volcanic centres during the shield building phase in the Pleistocene and the Holocene. Type I is described as having a microdoleritic groundmass containing phenocrysts of olivine ($Fo_{78-82}$), clinopyroxene ($En_{42-44}$) and plagioclase ($An_{70}$). Type II is described as having a basaltic groundmass with 50% of the rock containing microphenocrysts which include clinopyroxene ($En_{41}$) and fewer (3-15%) phenocrysts of olivine ($Fo_{71}$) and plagioclase ($An_{67}$) then type 1. Both Type I and II most likely originated from closely related magma chambers at different depths. (LeMasurier *et al*., 1990)

Type III is believed to have only erupted from the lesser western shield and to be a cumulate rock; it is described as basaltic rich in porphyritic plagioclase ($An_{82}$), with olivine ($Fo_{60}$) and clinopyroxene ($En_{37}$) being subordinate. Type IV is believed to have erupted from the eastern main shield and is a fluid-textured aphyric rock containing olivine ($Fo_{51}$) and clinopyroxene ($En_{34}$) with predominant laths of plagioclase ($An_{47}$) ( LeMasurier *et al*., 2012).

According to le Roex *et al.* (2012), interpretation analysis of the Marion island lavas indicated that they formed from relatively “simple petrogenetic processes”. It is further stated that perhaps the most notable feature of the lavas are the uniform isotope and incompatible element ratios as well as the simplicity of the compositional variations (le Roex *et al.,* 2012).

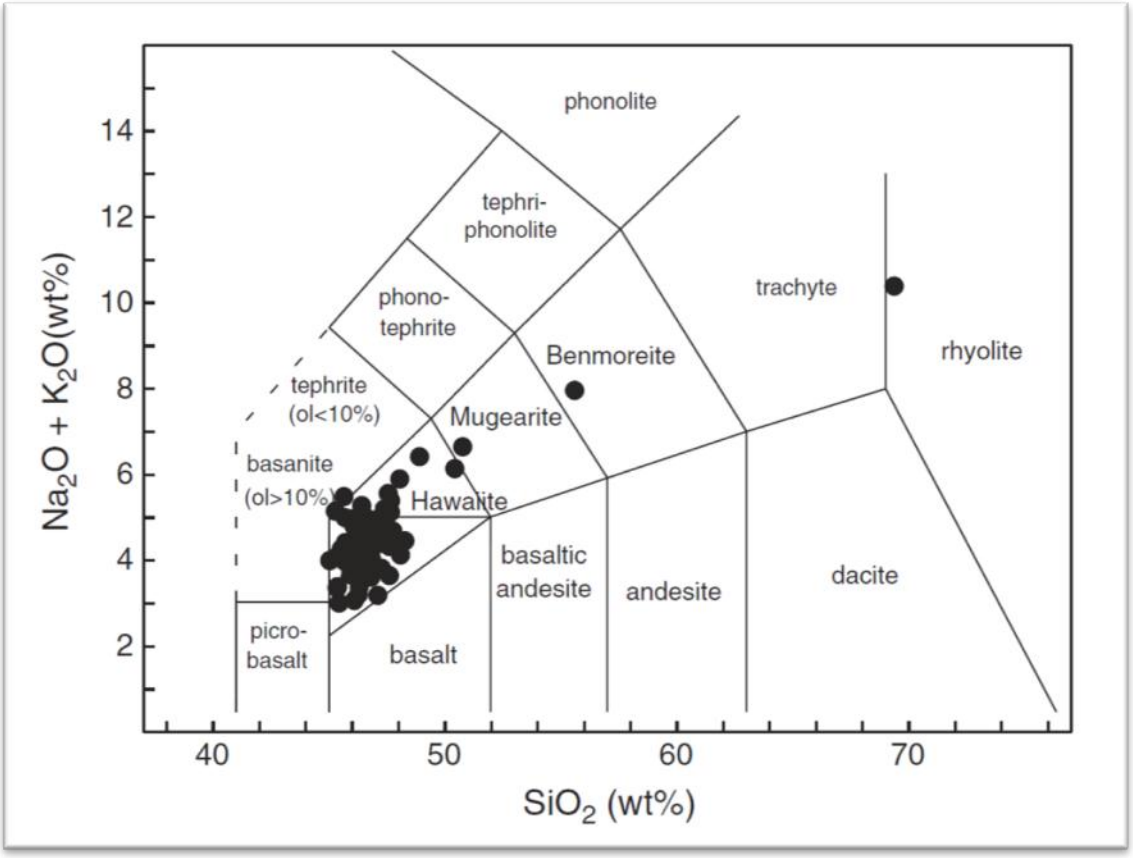


**Figure 4: From le Roex *et al.* 2012, total alkali-silica compositions diagram of Marion Island (90 samples)**

## *1.4 Clinopyroxenes*

In mafic volcanic rocks; clinopyroxene normally forms a significant part of the groundmass chemistry of ocean island basalts (OIB); however it is peculiar to find near perfect to perfect euhedral clinopyroxene crystals hosted in scoria (1 – 5 cm in size). In the case of OIBs it is common that the further the volcano drifts away from the hotspot the more clinopyroxene- and olivine- phyric the lava becomes (McBirney, 2007).

Clinopyroxene is a common mineral in mafic rocks. Clinopyroxene is a monoclinic inosilicate, with a large range of chemical compositions. The structural formula for clinopyroxene is $(M2)(M1)(Si,Al)_2O_6$ (Deer *et al.,* 1992). For the Ca-rich clinopyroxenes, $Ca^+$ has to occupy more than two-thirds of the

M2 site (Deer *et al.,* 1992). It is this occupation by the $Ca^{+}$ ion in the M2 site that causes a “kink” in the configuration of the chain of the inosilicate, thus changing the unit cell from orthorhombic to monoclinic (Deer *et al*., 1992).

When crystal growth occurs, the occupation of M1 and M2 sites are influenced by the pressure, temperature and chemical composition of the liquid (Deer *et al.,* 1992). Any change in any of these parameters will, however, slightly affect the preferential occupation of the ions in the different sites (Deer *et al.,* 1992). These occupation differences will lead to a variety of configurations in the chain configuration and is classified as zoning.

Clinopyroxene may display zoning, which is the focus of this study. According to Aydin *et al.* (2009), types of zoning can be related to crystallization of melts. Oscillatory and sectorial zoning can be related to crystallization of an evolving melt. Oscillatory and reverse zoning are related to different crystallization paths under the fluid regime. The enrichment of Al, Fe and Ti at the rims is indicative of normal zoning which are related to fractional crystallization of magma.

# Chapter 2: Sampling and Methodology

Sampling was done on the mid southern side of the island on a scoria cone named Pyroxene Hill (46˚56'36.29"S 37˚41'24.47"E) (Fig. 3). 3 kg of samples were randomly sampled from the scoria cone, selecting the least weathered, most euhedral and coherent crystals. Crystal sizes vary between 3 mm to 5 cm (Fig. 5).

**Figure 5: Photograph showing size distributions between the different clinopyroxenes and host scoria from Pyroxene Hill, Marion Island.**

Of these, ten crystals were selected and sent to the Council for Geoscience for mounting. The polished mounts were then analysed using a Joel 4800 SEM and the auxiliary Thermo scientific Noran System Seven EDS (Energy Dispersive Spectrometer) at 20 kV, in order to get the highest possible EDS resolution.

Compositions recorded by the EDS attachment during the SEM transect, indicated that there was a definite variation in chemistry. Analytical errors for the EDS analysis are given in Table 1.

**Table 1: Wt % estimated errors and lower level of detection as reported by EDS software.**

| Component Analysed | Wt % Error | Wt % Lower level of detection |
|---|---|---|
| O | 0.5 | 0.5 |
| Si | 0.2 | 0.5 |
| Ti | 0.1 | 0.5 |
| Al | 0.1 | 0.5 |
| Cr | 0.1 | 0.5 |
| Fe | 0.2 | 0.5 |
| Mg | 0.1 | 0.5 |
| Ca | 0.2 | 0.5 |
| Na | 0.1 | 0.5 |

Once this change in chemistry was noted, a backscatter study was done, using the Joel 4800 SEM inbuilt backscatter detector at 20 kV, on the crystal grains; however no zoning could be identified. Six samples were then selected for analysis by the Cameca X-100 microprobe operated at 20 kV and 20 nA . Widely spaced interval transects were then done on the six samples chosen. Following the results from the six samples, two were chosen for higher resolution (more closely spaced) transects. After one of these transects revealed a chemical variation over distance, the transect was extended further. All of this was done in one session without removing the samples from the probe, and without adjusting the original calibration of the probe since the start of the analysis so to have the analysis comparable to each other without having bias. Table 2 details the analytical errors for the microprobe analysis.

Once zones of significant chemical change were identified, the samples were again transferred to the SEM for higher detail backscattered imaging. The auxiliary Centaurus backscatter detector was used for imaging at 10 kV, and with these higher resolution images, slight distinction of grey-scale could now be identified. However the distinction was not significantly clear enough, so

further analysis was done by the Cameca factory in Paris, France utilizing a Cameca SX-Five FE microprobe field emission gun set up at 15keV, 60 nA, with a map area of 2200 X 1000 µm, resolution of 1101 X 501 pixels, 40 ms dwell time per pixel and a stage scan of 2 µm step. AS this instrument is still in development, only the images were supplied from this analysis, and details of the individual data points are not given in this study.

**Table 2: Estimated wt % errors, lower level of detection values (ppm) and wt %, as reported by microprobe software.**

| | | Lower limit of detection | |
|---|---|---|---|
| Component analysed | Wt % Error | Wt % | ppm |
| Si | 0.23 | 0.03 | 340 |
| Ti | 0.07 | 0.05 | 450 |
| Al | 0.09 | 0.03 | 310 |
| Cr | 0.06 | 0.05 | 490 |
| Fe | 0.17 | 0.05 | 480 |
| Mn | 0.04 | 0.05 | 470 |
| Mg | 0.51 | 0.03 | 300 |
| Ca | 1.09 | 0.04 | 410 |
| Na | 0.03 | 0.01 | 130 |

# Chapter 3: Results

Scanning electron imaging revealed that the clinopyroxene crystals have several fractures and tend to be pitted, probably due to the polishing process as well as some inclusions (Fig. 6 and 7). The crystals contain olivine inclusions as well as microscopic sulphide and spinel inclusions which were qualitatively, but not quantitatively analysed by EDS. The sulphide inclusions are present in both the olivines and the clinopyroxene. The crystals in total contain approximately 10% inclusions (of sulphides, spinels and olivines).

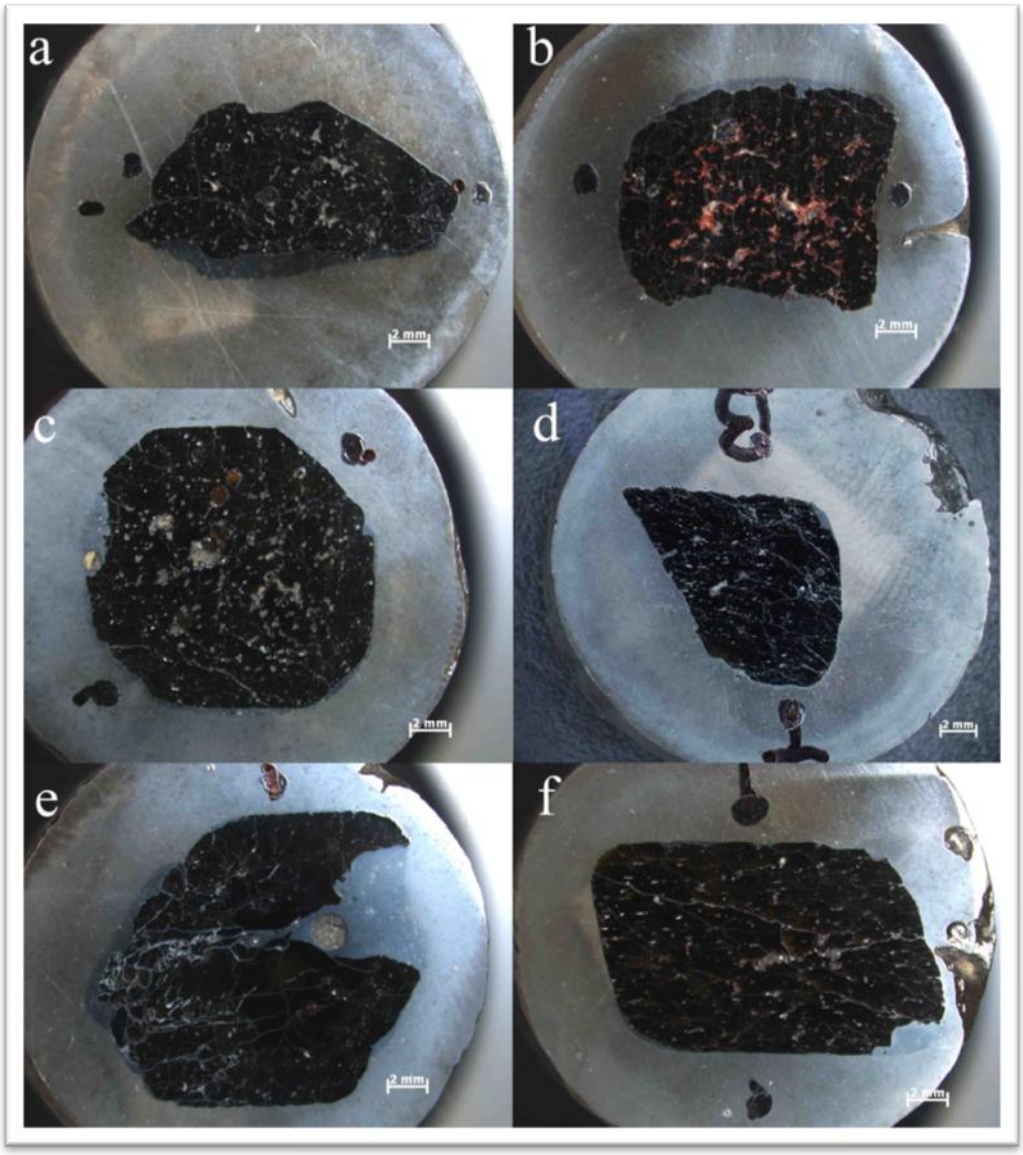


**Figure 6: The six sample mounts selected for microprobe analysis. a) Sample 2, b) Sample 4, c) Sample 5, d) Sample 6, e) Sample 9, f) Sample 10.**

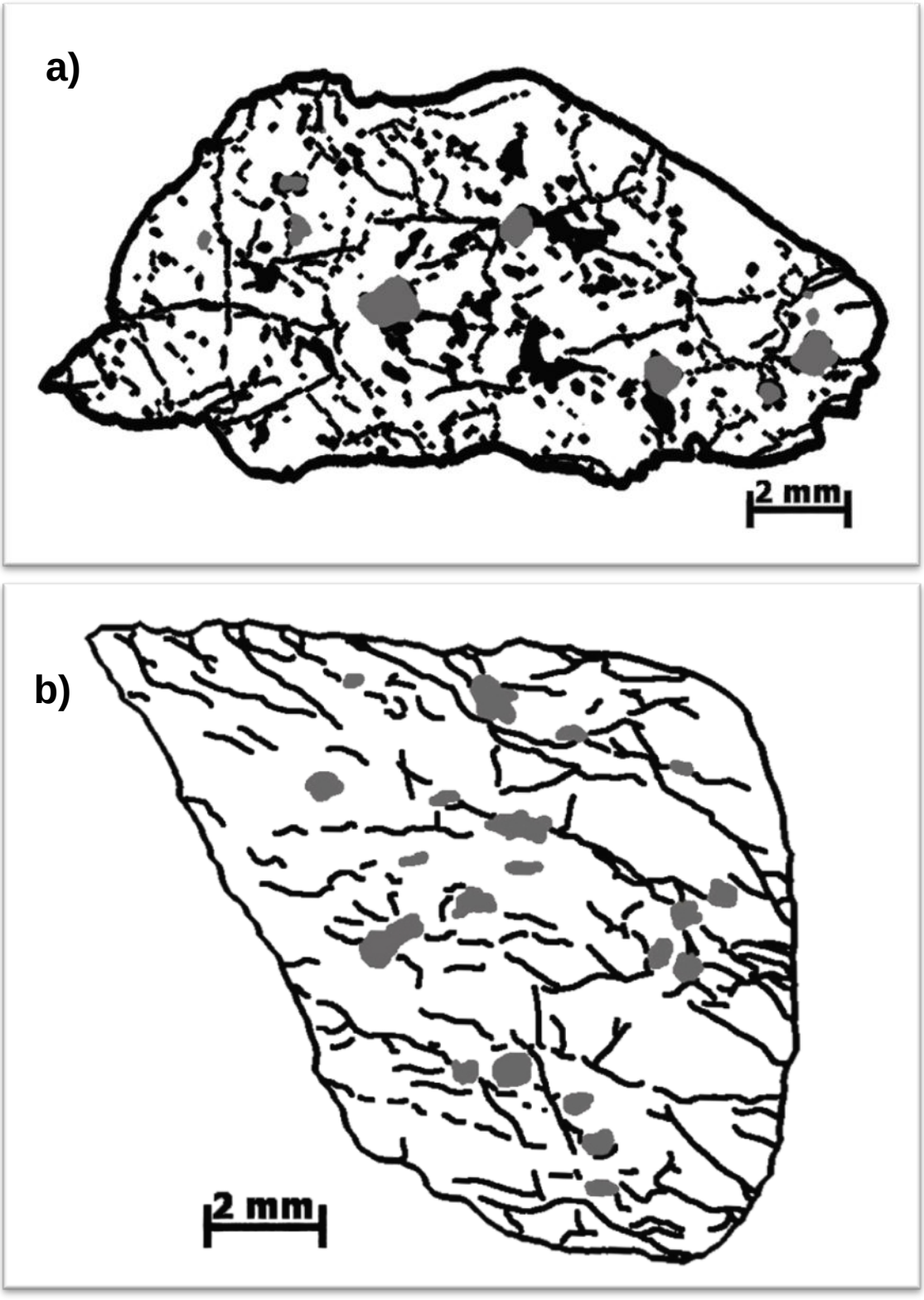


**Figure 7: Sketches of sample 2 (a) and 6 (b), grey indicate macroscopic olivine inclusion and the black lines indicate cracks and pits in the crystal.**

Preliminary EDS results (appendix I; summarised in Table 3) showed that the crystals are not homogenous and that there is a change in chemistry from core to rim (Fig. 8) and appear to have some form of grouping. However the $Cr_2O_3$ and $TiO_2$ results are indicative of elemental presence, but owing to the lower level of detection (Table 2) on the EDS of the SEM, this data is speculative at best (with lower level of detection limit restricted to >0.5 wt %)

**Table 3: Summarised max and min EDS results (Appendix I)**

| Component Analysed | Min Wt % | Max Wt % |
|---|---|---|
| O | 40.9 | 45.1 |
| Si | 22.5 | 25.5 |
| Ti | < LLD | 1.5 |
| Al | 1.2 | 4.0 |
| Cr | < LLD | 0.9 |
| Fe | 3.9 | 6.0 |
| Mg | 7.9 | 11.1 |
| Ca | 13.9 | 16.0 |
| Na | < LLD | 0.7 |

The Joel 4800 backscatter images did not show any significant zoning or banding, in any of the 10 mounts, which would explain the suspected change in chemistry from the core to the rim. It was thus possible that the suspected heterogeneity of the crystals was on too small scale to be detected by the inbuilt backscatter detector, or that the EDS results reflected the inherent analytical error of the EDS. As the concentration of the elements of interest was below a level at which detection would be statistically quantitative, no further EDS data was captured. The higher resolution of a microprobe (as much as an order of magnitude higher) was needed to determine whether the suspected chemical variance was a function of the EDS analytical error or reflected actual chemical variation.

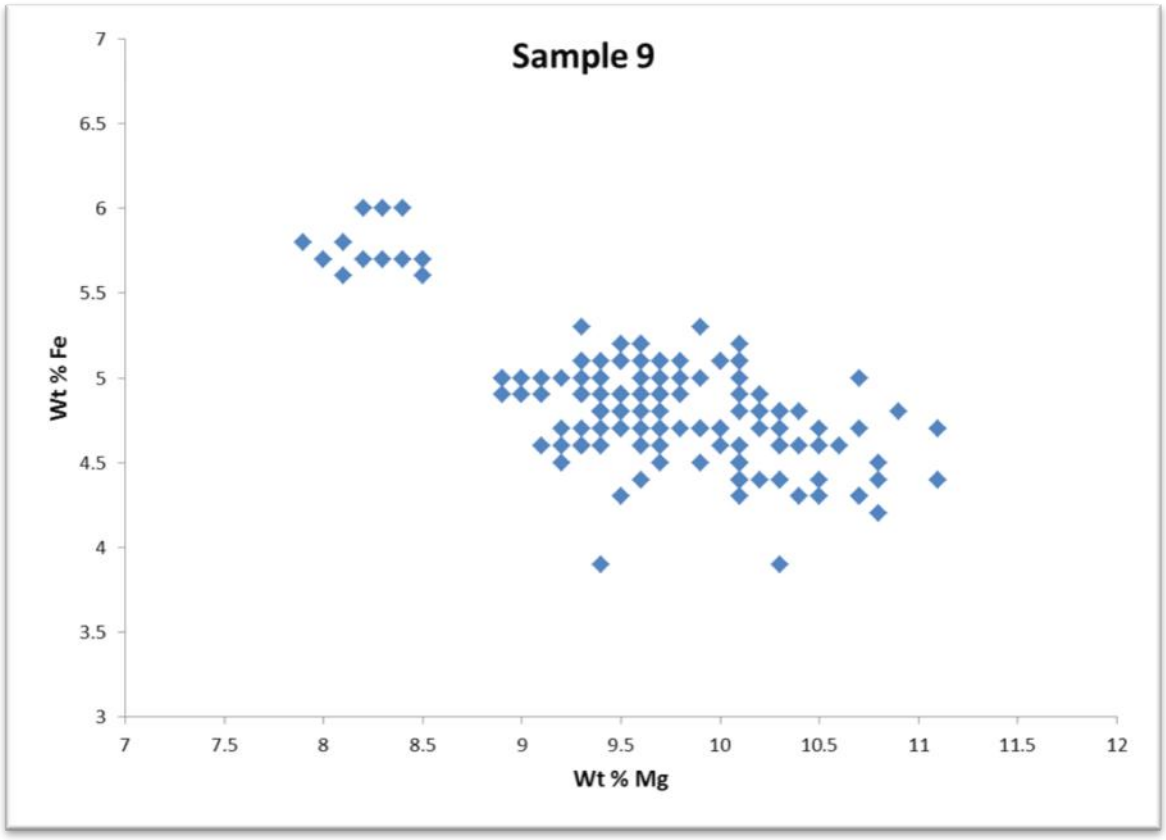


**Figure 8: Sample 9 EDS data, plotting Mg vs. Fe wt %.**

Because of restricted resources, only six of the original 10 mount could be analysed by the microprobe. The six mounts chosen randomly can be seen in Figure 6. Large interval transects (approximately 330 to 500 µm intervals respectively) were done on each of the six samples. The result from the larger interval microprobe transects revealed differences in chemistry, resembling that which one would expect from zoning or banding of crystals (Fig. 9). Resources permitted us to run a second set of analysis on selected parts of two of the samples with smaller interval transects (at approximately 14 µm intervals). Sample 2 and sample 6 were selected for the smaller interval transects. These finer transects done on the microprobe (Fig. 10) then showed results very similar to that seen in Morgan *et al.* (2004) and Nakagawa *et al.* (2002), in that spatial variations in composition supported the zoning or banding theory. The MgO content exhibits an inverse relationship to the $TiO_2$ (Fig 11).

Knowing the approximate areas of chemical change, the two samples (samples 2 and 6) were again analysed by the SEM; however this time a finely tweaked Centaurus back scatter detector was used at 15kV, (The auxiliary Centaurus backscatter detector is capable of detecting smaller compositional changes in the crystal than the built-in backscatter detector of JOEL 4800). The grey-scale shading reveals an irregular texture which does hint towards more complex zoning than regular, oscillatory or reverse zoning (Fig. 12). The backscatter image can be interpreted as showing an irregular core which does not look like the result of normal concentric, oscillatory or sector zoning. Nevertheless the field of view remains a limiting factor, and, coupled with low contrast in the greyscale of the image, makes for very weak speculation at best. For a larger field of view and compositionally representative mapping, microprobe mapping was used (Fig. 13).

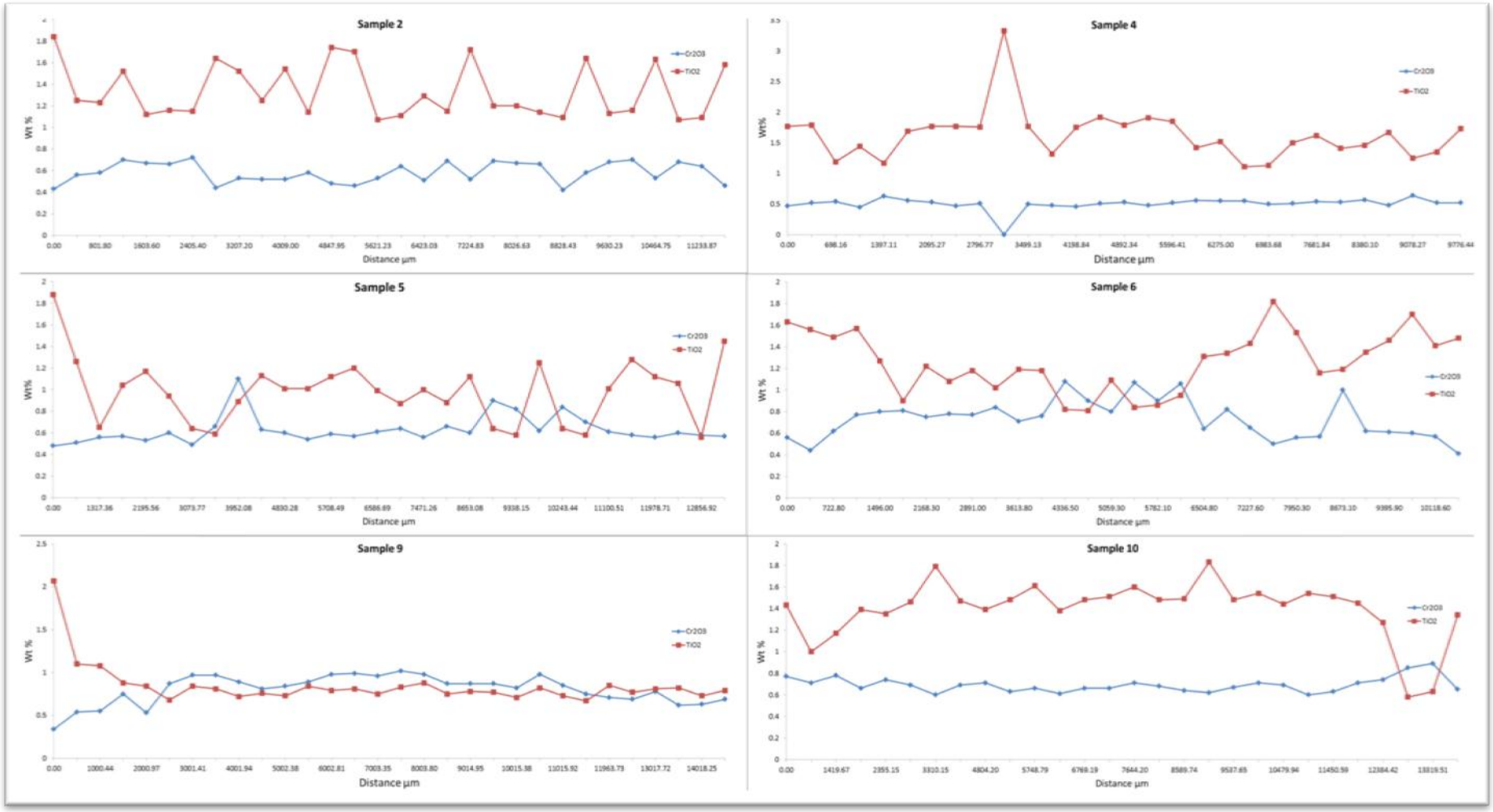


**Figure 9: The six large interval transects done by microprobe on the clinopyroxene mounts (blue line represents $Cr_2O_3$ wt % values and red line represents $TiO_2$ wt % values). The Cr2O3 values has an error margin of 0.06 wt% and the TiO2 values has an error margin of 0.07 wt%. The LLD for both values are 0.05 wt%.**

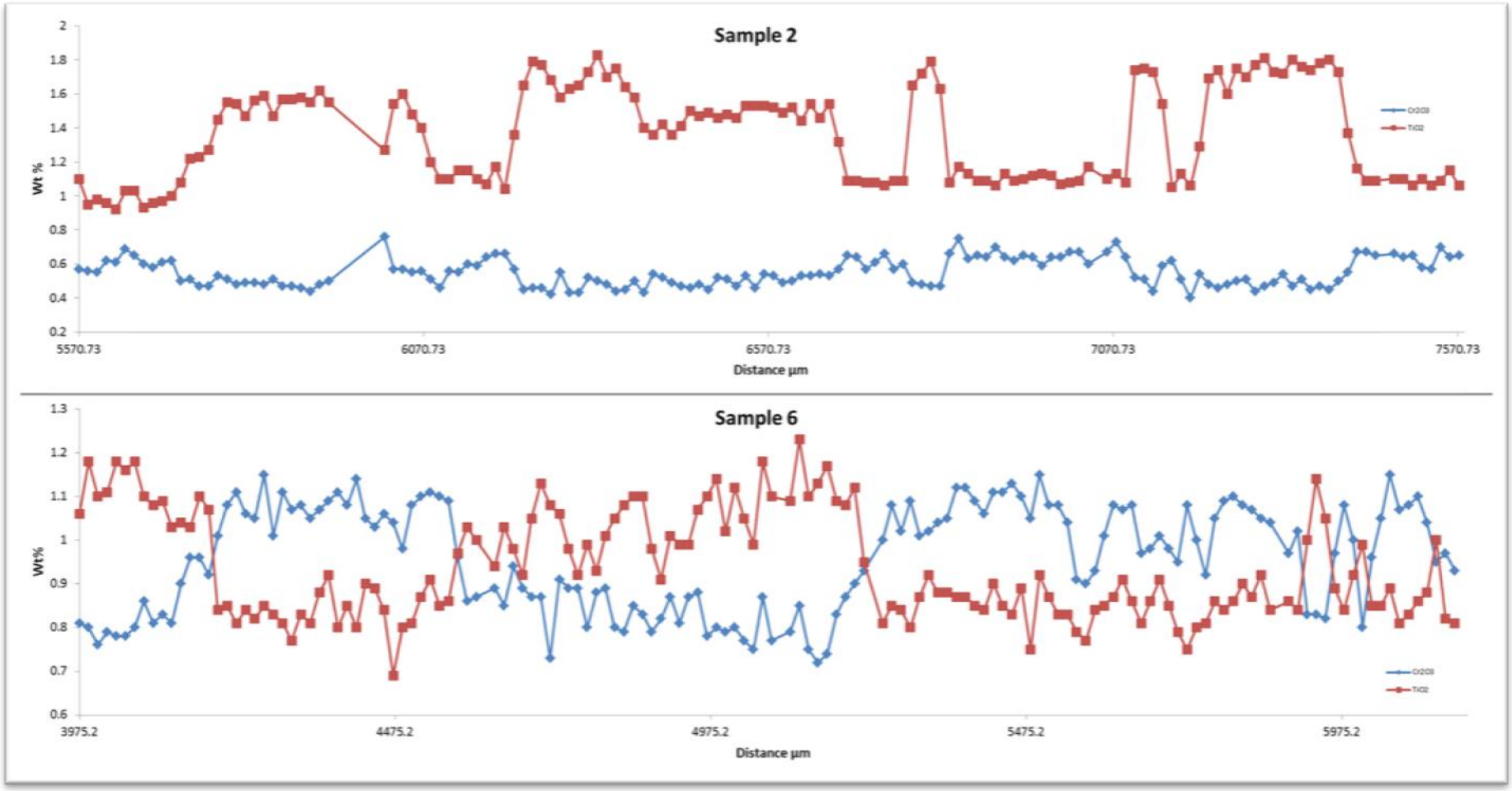


**Figure 10: Smaller interval transects done by microprobe (Appendix III), revealing very similar pattern to that which can be seen in Morgan et al. (2004) and Nakagwa et al. (2002). The Cr2O3 values has an error margin of 0.06 wt% and the TiO2 values has an error margin of 0.07 wt%. The LLD for both values are 0.05 wt%.**

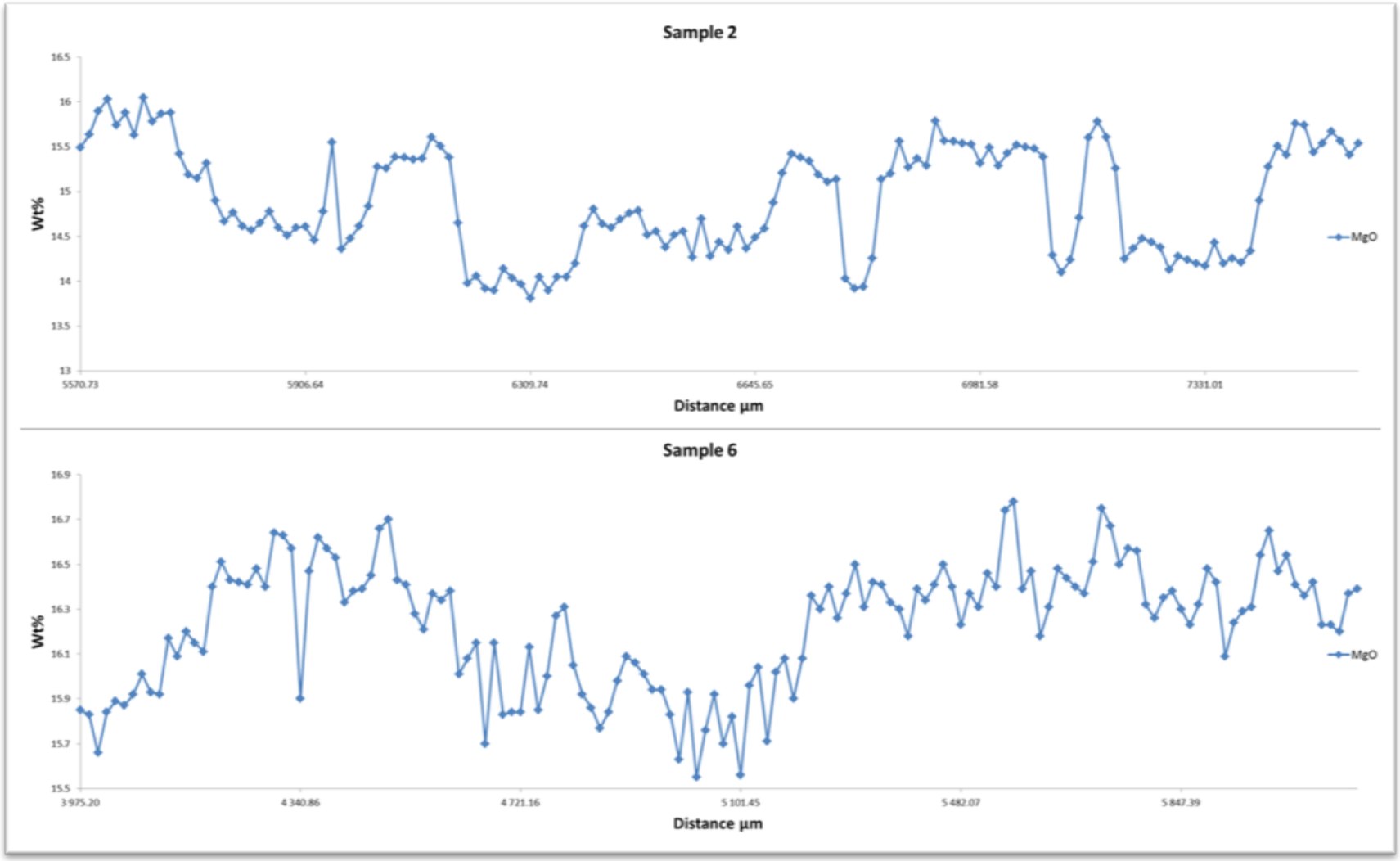


**Figure 11: Small interval transects of MgO across sample 2 and 6, (microprobe results). The MgO values has an error margin of 0.51 wt%. The LLD values are 0.03 wt%.**

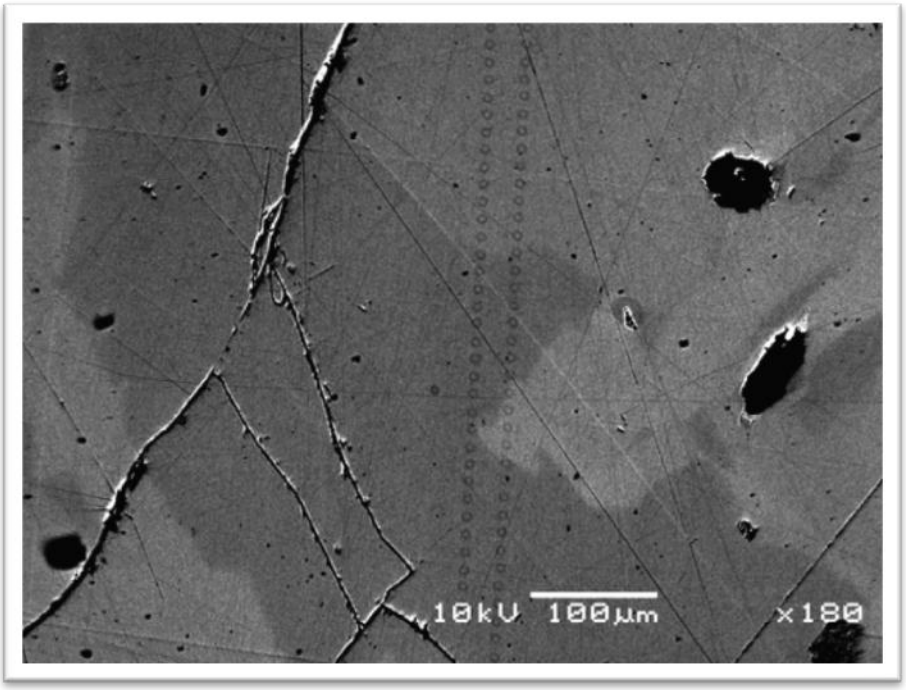


**Figure 12: Centaurus backscatter image of samples 6, the two rows of dots visible are the tract of the microprobe**

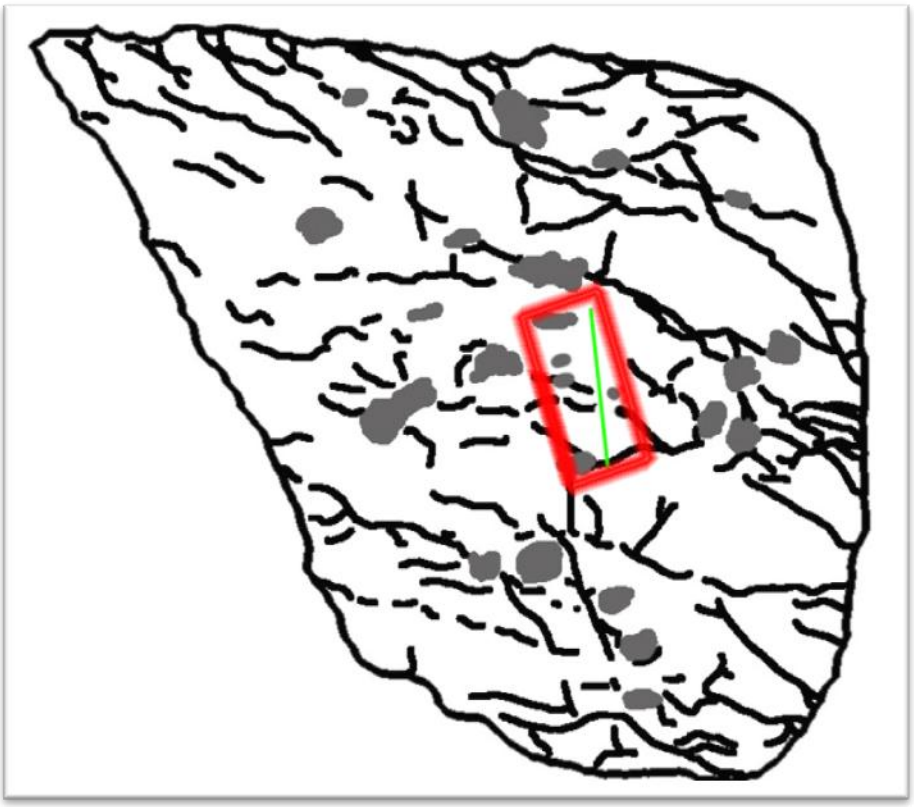

**Figure 13: Sample 6 with the red block showing Cameca mapped area and green line showing small interval transect line. Black lines indicate cracks and boundaries of the crystals, and grey patches indicat pits and inclusions.**

The Cameca chemical composition distribution maps provided the best image of the chemical distribution in the crystal as well as field of view (Fig. 14, 15, 16, 17, 18 & 19). Only one sample could be analysed using this technique, and thus the sample with the highest probability of showing zoning patterns were chosen. From the smaller interval microprobe transects, sample 6 was chosen. The resulting images from sample 6 show a very complex zoning pattern, with sharp boundaries at some sites and more diffuse boundaries at other sites. It is also possible to roughly divide the zoning into three groups based on the shading difference observed (as seen in Fig. 20).

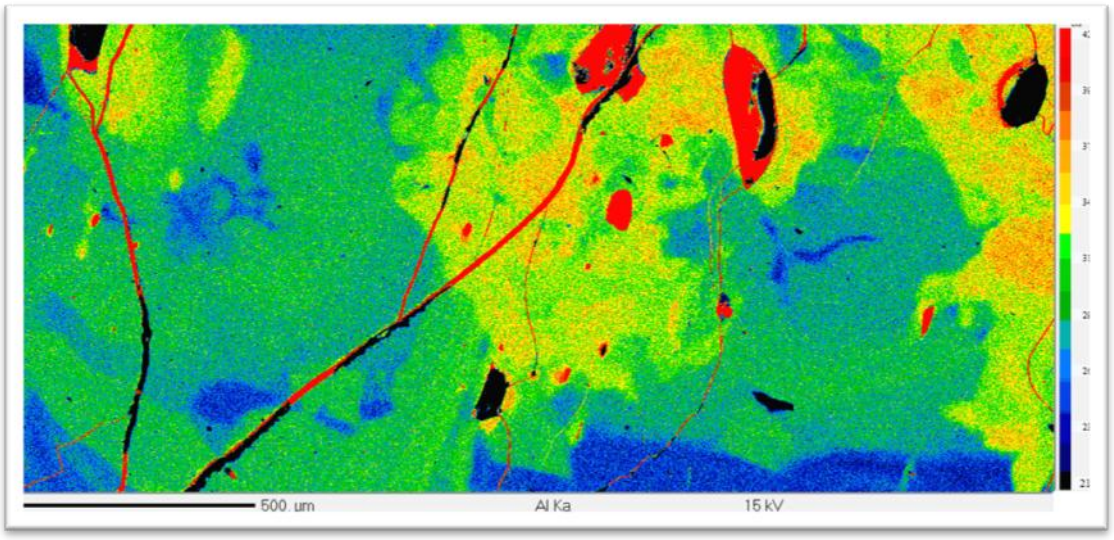


**Figure 14: Sample 6 Cameca SX 5 FE Micro probe Al Kalpha map at 15 kV, 60 nA.**

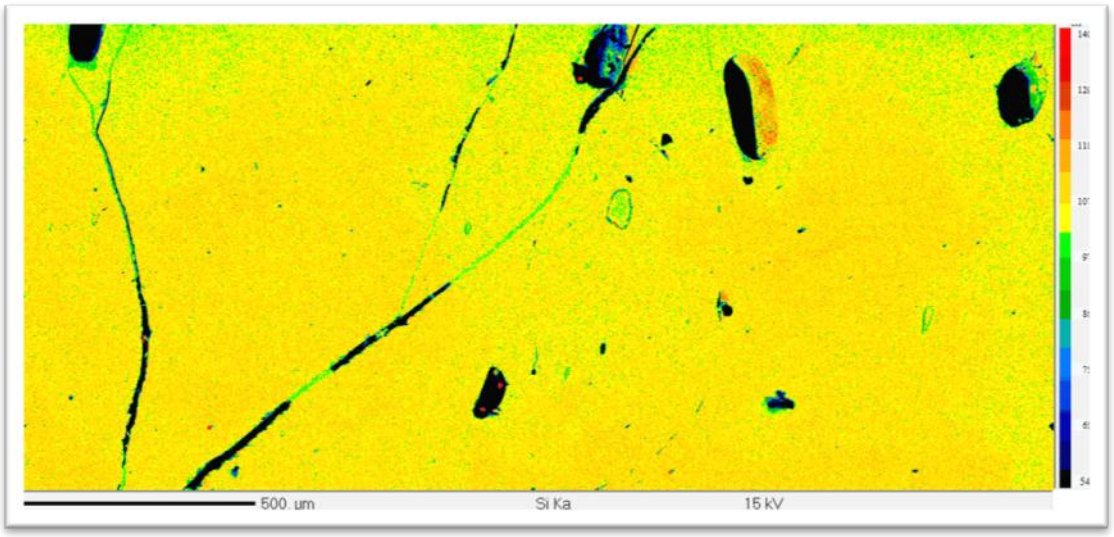


**Figure 15: Sample 6 Cameca SX 5 FE Micro probe Si Kalpha map at 15 kV, 60 nA**

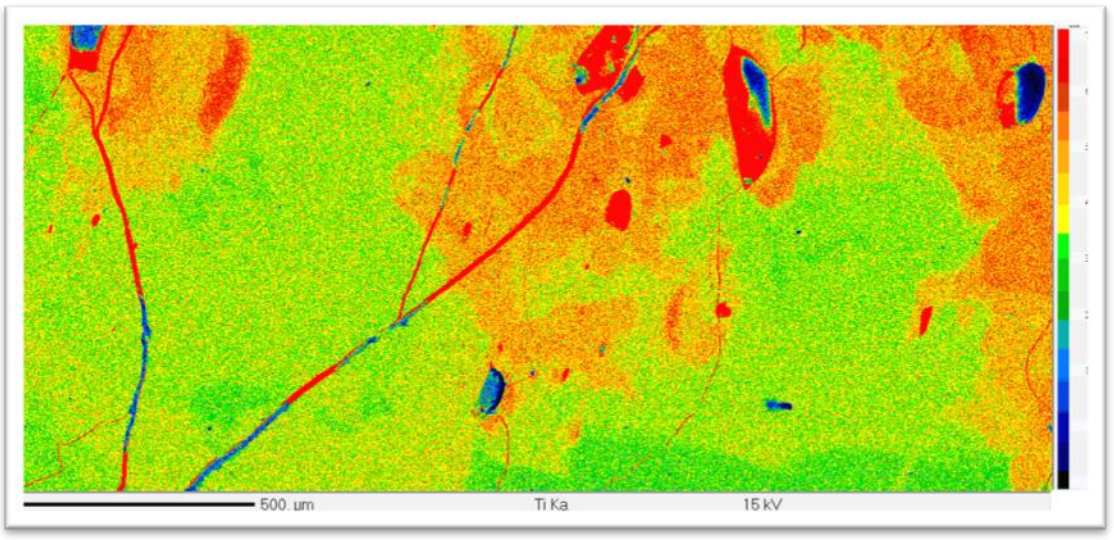


**Figure 16: Sample 6 Cameca SX 5 FE Micro probe Ti Kalpha map at 15 kV, 60 nA**

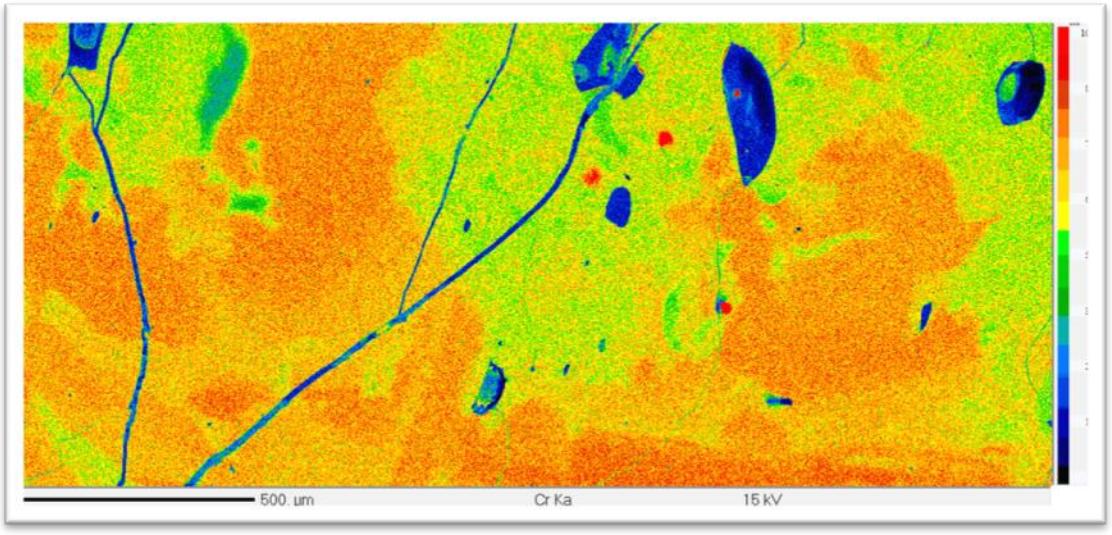


**Figure 17: Sample 6 Cameca SX 5 FE Micro probe Cr Kalpha map at 15 kV, 60 nA**

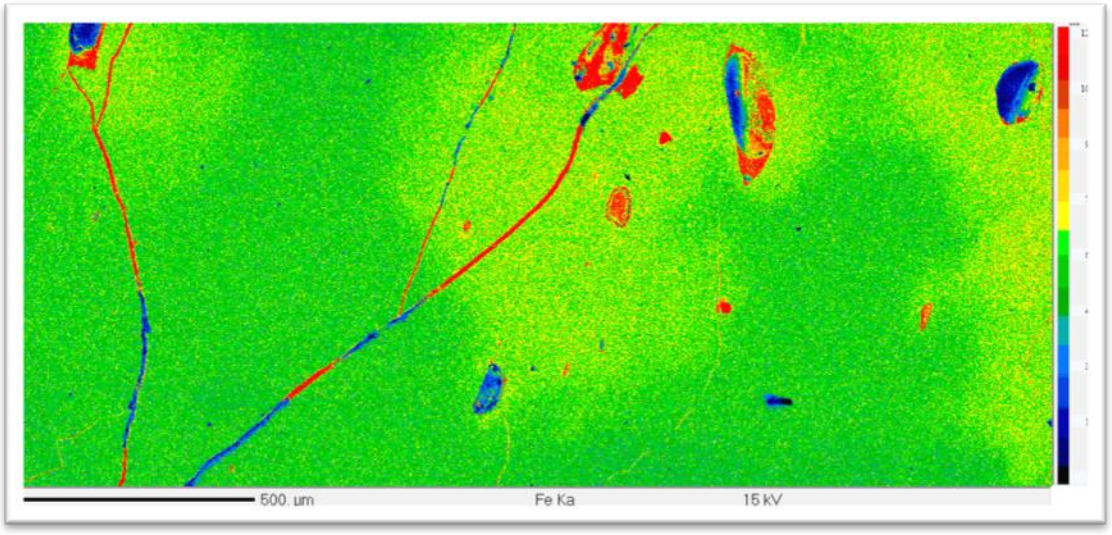


**Figure 18: Sample 6 Cameca SX 5 FE Micro probe Fe Kalpha map at 15 kV, 60 nA**

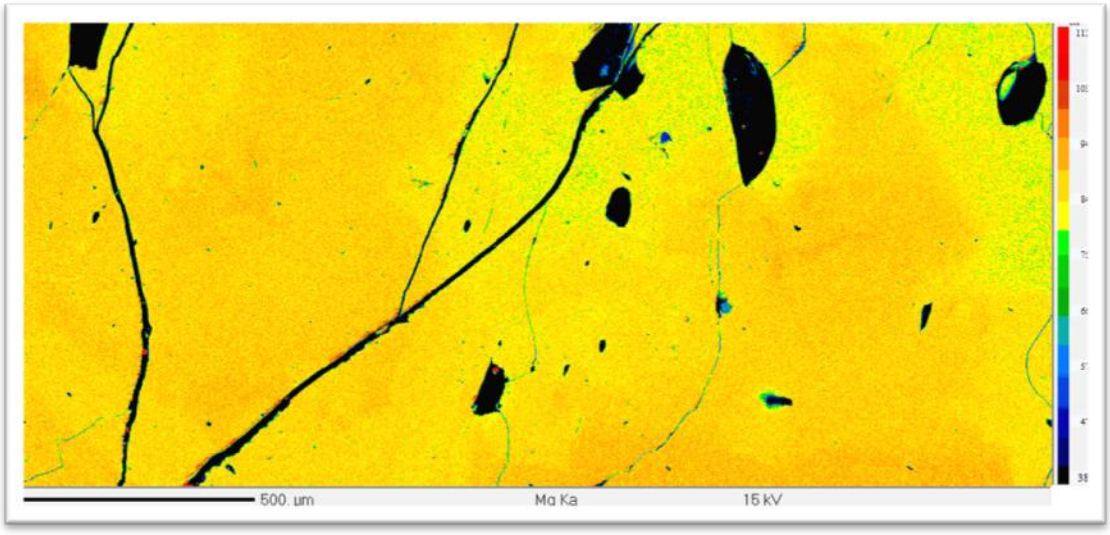


**Figure 19: Sample 6 Cameca SX5 FE Micro probe Mg Kalpha map at 15 kV, 60 nA**

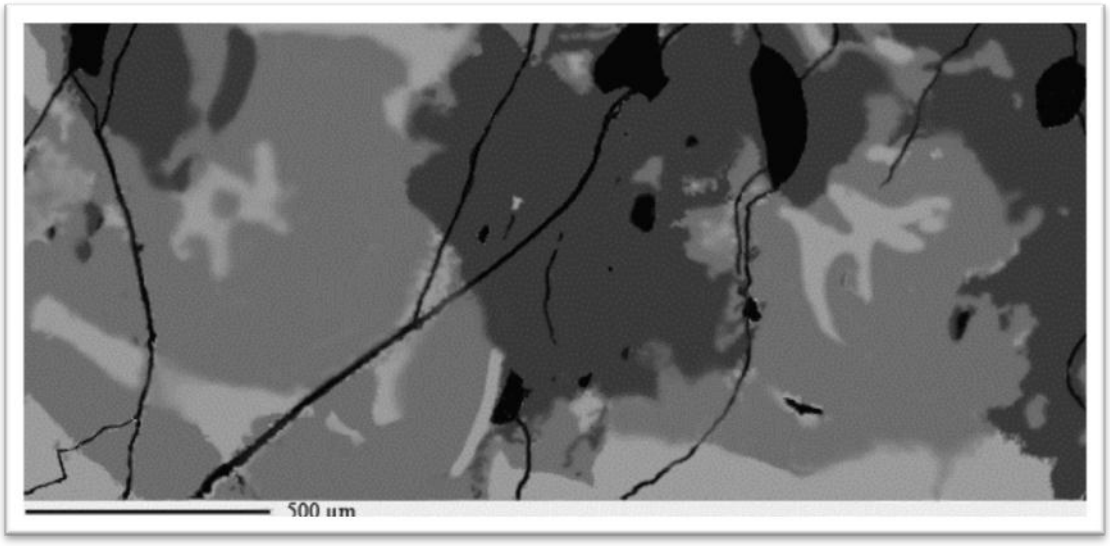


**Figure 20: Sketch of combined Cameca images of sample 6, roughly illustrating the suspected three different zones. Some of the boundaries between the layers are sharp and others are more gradual.**

Plotting the microprobe data as per formula unit (pfu) on a Mg – Fe – Ca triangle diagram (Fig. 21) show the geochemical distribution of the clinopyroxene crystals to be mainly diopsidic and some as augite. The majority of the clinopyroxene crystals have a Ca (Wo) content between 45 – 50% , Mg (En) content between 40 – 55% and a Fe (Fs) content between 5 – 10%.

The geochemical data from the microprobe analyses of sample 6 (the same crystal analysed in Cameca microprobe maps) are plotted on Figures 22, 23 and 24, in wt % oxide. The variation in the MgO/FeO/$TiO_2$ ratio is clearly visible in Figure 22, and it can be seen that the data fall roughly into three groups. Individual crystals are not homogenous- sample 6, for example, shows high MgO and low MgO (relatively) areas. The linear array visible in Figure 22 is a result of the distribution of Mg and Fe cations within the clinopyroxene lattice. Figure 23 and 24 shows the $Cr_2O_3$ distribution amongst the crystals, and, again, groupings within the data indicate clearly that the crystals are not homogenous.

The large interval data set was recalculated to ‘per formula unit’ (pfu) which was plotted against Aydin et al. (2009) clinopyroxene geobarometer (Fig 25). The results were ambiguous with the data plotting in overlapping fields. The Nimis and Taylor (2000) model was then used with sample 6’s small interval transect data. The model was set up with a proposed melt temperature of 1200k which produced a variation in crystallisation pressure ranging from the crust to mantle.

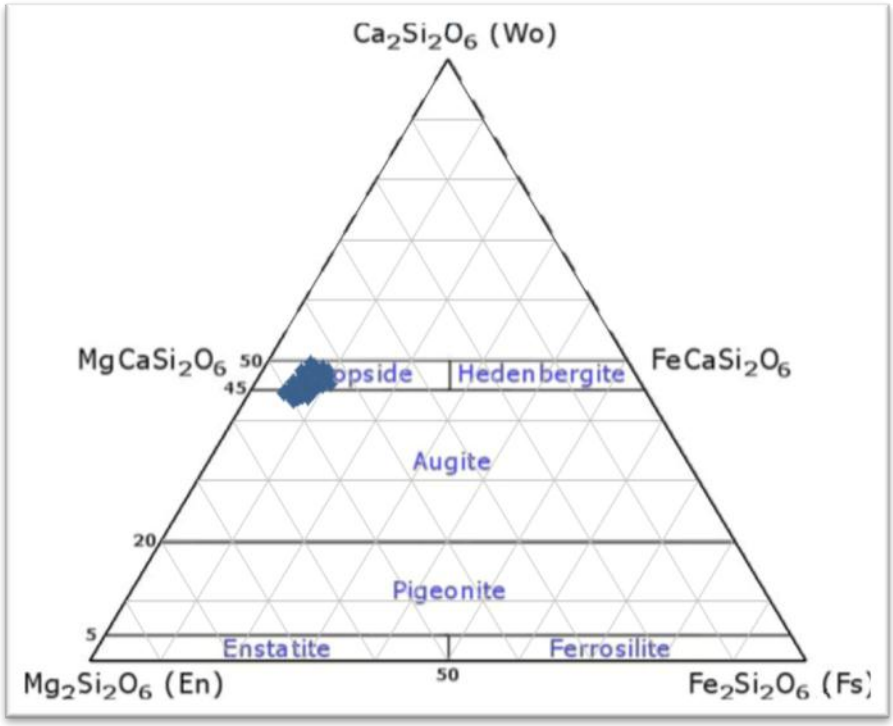


**Figure 21: Triangle plot to show the distribution of microprobe analysis from large interval transects of all six samples.**

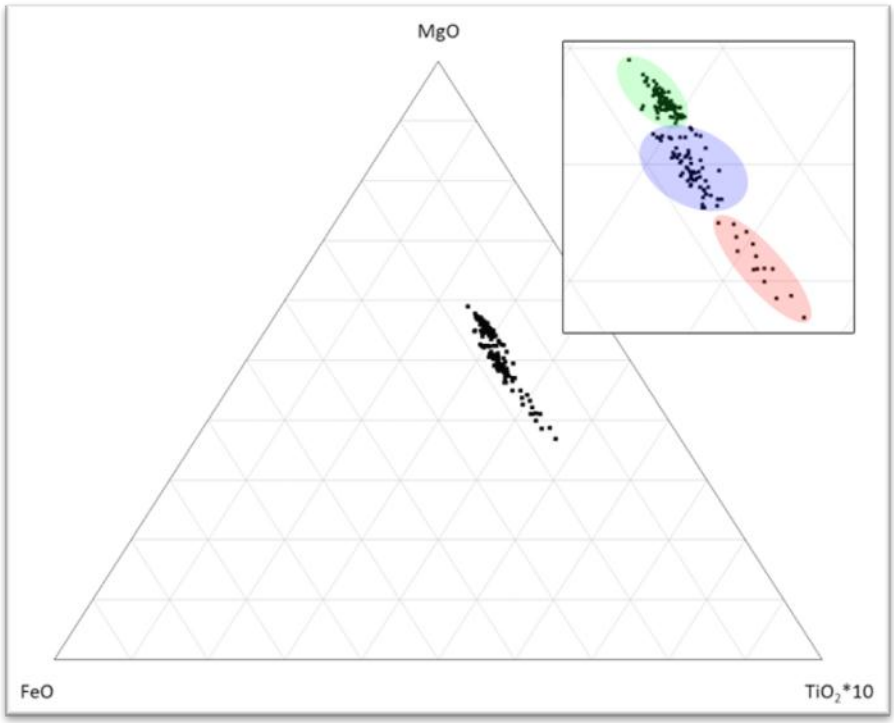


**Figure 22: MgO, FeO and $TiO_2$*10 triangle plot of small interval transect microprobe data from sample 6, showing three groupings of the data.**

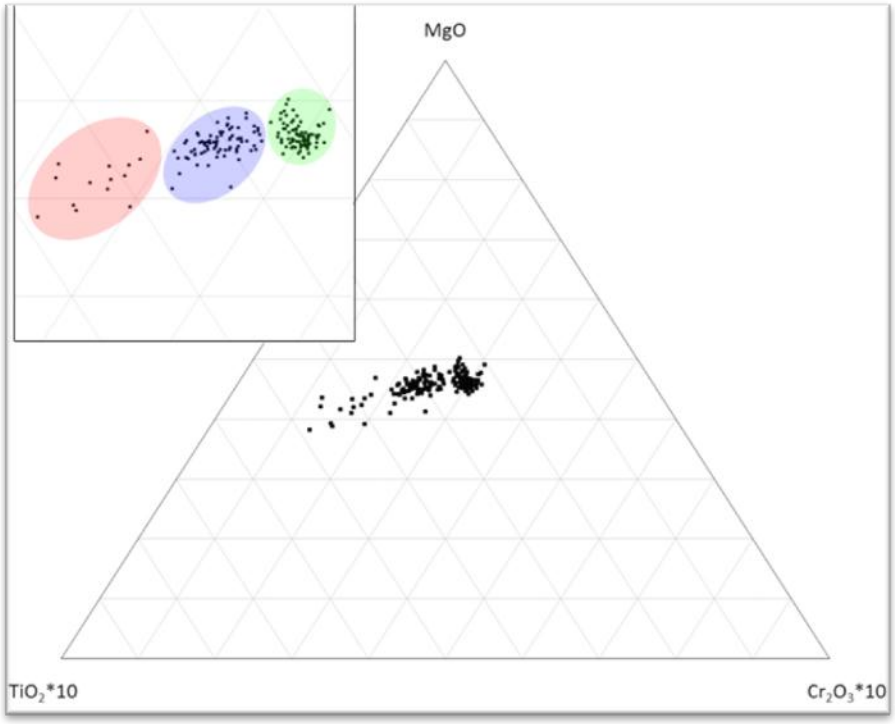


**Figure 23: MgO, $TiO_2$ and $Cr_2O_3$ triangle plot of small interval transect microprobe data from samples 6, showing three groupings of the data.**

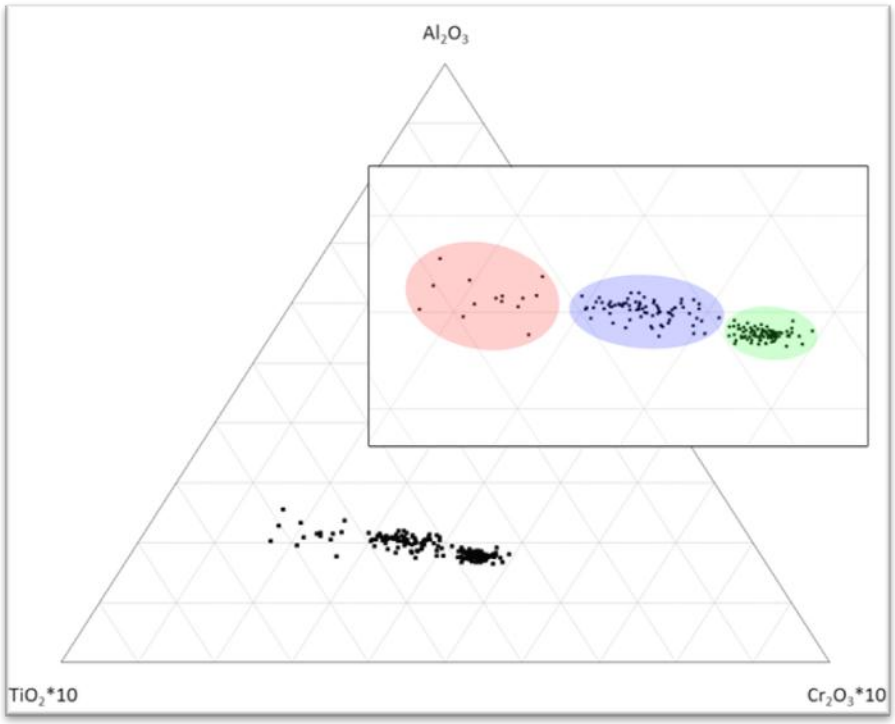


**Figure 24: $Al_2O_3$, $TiO_2$ and $Cr_2O_3$ triangle plot of small interval transect microprobe data from sample 6, showing three groupings of the data.**

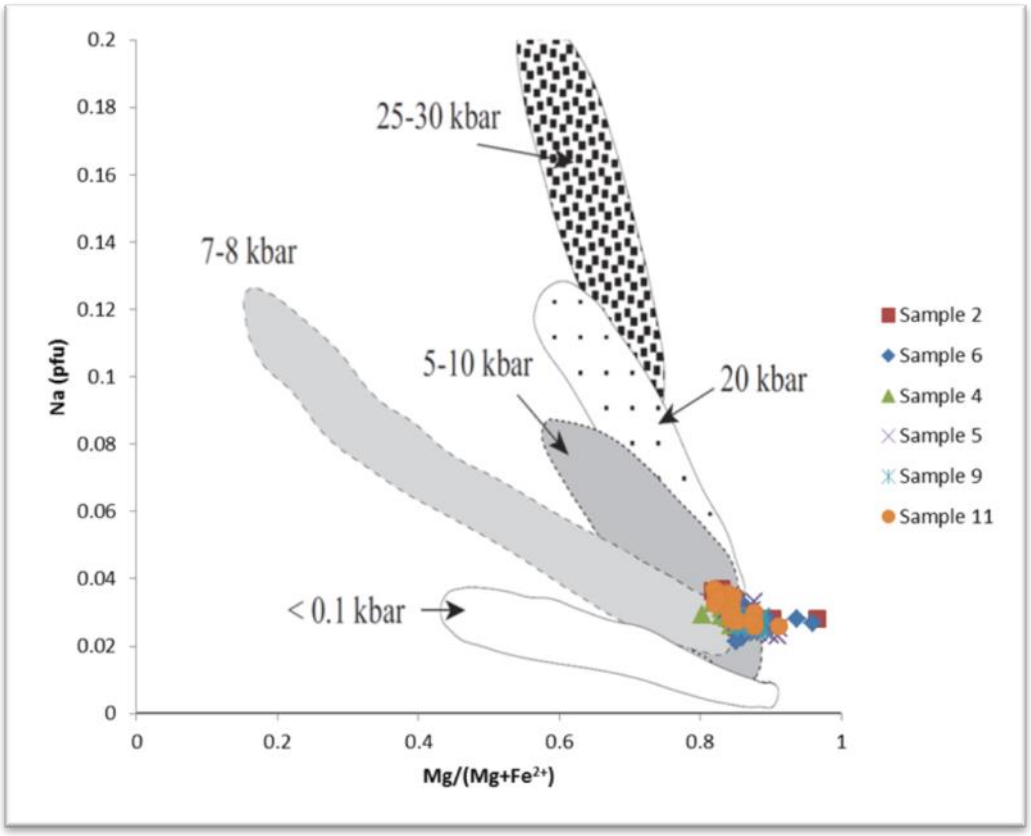


**Figure 25: Binary plot of Na vs. Mg/($Mg^{+}$+$Fe^{2+}$), by per formula unit, based on Aydin et al. (2009) showing distribution**

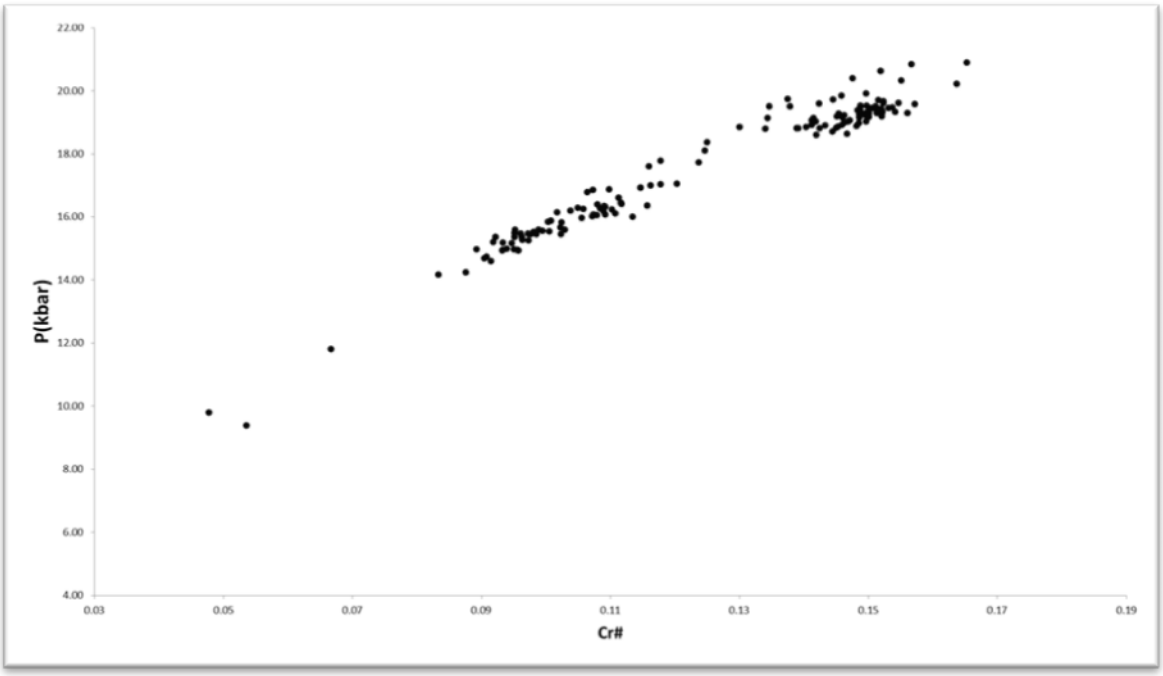


**Figure 26: Sample 6 small interval transect modelled using Nimis and Taylor (2000) Single clinopyroxene geobarometry.**

# Chapter 4: Discussion

## *4.1 Zoning in the Marion clinopyroxene megacrysts*

Zoning in crystals may imply a change in the local parameters of the magma environment at the time of crystal growth. These parameters may be pressure, temperature and compositionally related, and any change in one of these parameters could result in the formation of zonation in the crystal (Shore and Fowler, 1996). Zoning in minerals could be indicative of an open system, a reasonable assumption for a magma chamber undergoing periodic eruption and refilling as it fractionates. Zoning in clinopyroxene crystals is often preserved in magma bodies, thus need not only confined to low-temperature or rapidly grown and cooled paragenesis (Shore and Fowler, 1996).

Normal zoning can be defined as the compositional change from core to rim of a crystal along its liquid line of descent (Streck, 2008). This zoning pattern would tend to follow the crystal growth faces (thus mimic the euhedral shape of the crystal). The boundaries in normal zoning can be step like but diffusion may occur if the crystal is given enough time in the magma chamber, resulting in a more gradual change between zones (Morgan and Blake, 2006). According to Tomiya and Takahashi (2005), normal step zoning can indicate more complex growth coupled with open system processes. For a closed system a more gradual change would be expected rather than a sharp step-like change, as the concentrations of the absorbed components in a closed system would gradually decrease or increase depending on the crystallisation sequence. In the case of an open system any change in the pressure, temperature and/or composition is likely to be recorded in the crystal as a more abrupt change.

In the case of clinopyroxene, normal zoning would require a gradual or step-like compositional change in magma composition, specifically a decrease of Mg and Cr and an increase of Mn and Ti (Streck, 2008). This does not appear to have happened in the case of the Marion megacrysts. Fig. 12 indicates that the crystals are not normally zoned, as the Mg content increases and decreases seemingly sporadically. This contradicts to the requirement of normal zoning that a gradual or step-like decrease of MgO is needed (Fig. 11). $Cr_2O_3$ and $TiO_2$ also follow the same sporadic trend as Mg; however Ti has the inverse trend to that of MgO and $Cr_2O_3$.

Reverse zoning is compositionally inverse to normal zoning, therefore contradictory to what would be expected from the normal liquid line of decent, and thus what one would not expect to find in closed system crystallisation (Streck, 2008). Hence reverse zoning can be defined as the compositional change from core to rim contrary to the liquid line of decent. Reverse zoning can tend to mimic the euhedral shape of the crystals (follow the crystal growth faces) or can be anhedral to the expected crystal growth faces.

In clinopyroxenes reverse zoning can be very common (Streck, 2008). They can be present as bands which can be located anywhere between the core and the rim. These bands can occur several times in a single crystal repetitively, which would according to Streck (2008), suggest the injection of more mafic magmas into the magma chamber, which in turn causes multiple growth events. Mg and Fe do, however, not need to follow the traditional reversed chemical trend to normal zoning, and the injection of new mafic magma can correlate positively to Cr trends. An influx of a more Fe-rich magma into a Mg-rich mafic magma can result in mixing and a spike in Cr content (Streck, 2008)

However the zoning in the Marion crystals does not adhere to the definition of reverse zoning any more than it does to normal zoning. Although reversely zoned banding can have irregular shapes, the general chemistry is still too sporadic for reverse zoning to apply. The MgO and $TiO_2$ (Fig. 13 & 24) do have a strong inverse correlation, but represent normal zoning followed by reverse zoning in no specific order. Reverse zoning being inverse to what would be expected from a closed system (Streck, 2008), one would expect to have a more gradual compositional changes in chemistry between zones. However the changes seen in the crystals (Fig. 14 – 20) show gradual changes as well as sharp step-like changes or banding, often on the same zone boundaries.

Oscillatory zoning was defined by Shore and Fowler (1996) as growth-shells or layers of varying composition that can have a range of thicknesses of between tens of nanometers to several tens of micrometers; furthermore these bands would generally be parallel to the crystallographic planes of low Miller indices and be concentric to the external margins of the crystal. Regular and harmonic composition and thickness in zoning fluctuations are not needed for oscillatory zoning (Shore and Fowler, 1996). Chemically oscillatory zoning is generally just normal zoning that repeats and varies over short distances (Shore and Fowler, 1996)

.

Holten *et al.* (1997) divide the general assumptions of how oscillatory zoning works into two types: (a) those created by internal growth processes in the crystals, or (b) those zoning patterns reflecting large scale changes in external geology (i.e. magma chamber conditions). Streck (2008) then suggest that oscillatory zoning be subdivided into “fine banding” and “coarse banding” based on zoning width. It was hypothesised that fine banding (on the scale of single microns, 1-10 µm) in clinopyroxenes may reflect small scale composition changes or oscillations, and this is believed to be largely kinetically controlled (Streck, 2008).

In the clinopyroxene crystals from Marion Island, the zoning appears not to follow any form of oscillatory pattern to the euhedral outline of the crystals. The zoning or change in chemical distribution tend to diffuse at certain areas and be abrupt at others (Fig. 9 & 20). The high resolution Cameca images also do not indicate any form of oscillatory zoning at the scales indicated by Streck (2008).

Sector zoning in a single crystal is a form of zoning in which each crystallographic sector has its own distinct chemistry (Dowty, 1976). The different growth sectors are best envisioned as pyramid-like in form with the peak of the pyramid at the centre or origin of the crystal and the base at the face of the crystal (Dowty, 1976).These sectors form surface kinetic processes, i.e. preferential absorption-desorption of ions of different charges and electro negativities in different growth sectors during crystallization (Aydin et al, 2009). This would be a function of extremely localised inhomogeneity in the liquid surrounding the crystal, where the different crystal-liquid boundaries become enriched and depleted in certain ions during the crystal building process.

In clinopyroxenes, sector zoning is assumed to be a metastable phenomenon (Hollister, 1996). As a result of this metastable growth process all Ti, Al and $Fe^{3+}$ are incorporated into sectors with the most M1 sites thus areas with highest acceptability for these ions, whereas the {110} sectors of the crystal only have M2 sites (which are generally saturated with Ca) (Dowty, 1976 and Hollister and Gancarz, 1971).

The Marion samples show no such sector zoning pattern. Although there is substitution of Si with Al and $Fe^{3+}$, the distribution of this geochemical variance does not appear to be in sector-related patterns. The crystals thus do not show any relationship between the chemical variation and the crystal morphology, despite the roughly euhedral morphology of the crystals. The zoning can thus best be defined as “patchy”.

“Patchy” zoning in crystals are identified as where the zoning patterns are irregular (Vance, 1965). When referring to crystals as having patchy zoning, the implication is that normal and reverse zoning compositional variation are difficult to establish (Streck, 2008). Patchy zoning can be formed in one of two ways; if the crystal went through diffusion in the process of re-equilibration, or as a result of melt crystallising into the cavities of a skeletal crystal, in which case the new crystallisation needs to of a different composition (Streck, 2008). Distinguishing between diffusional re-equilibration and crystal growth as the origin for patchy zoning can be done on basis of the sharpness of compositional change between different patches. According to Stewart and Pearce (2004), a sharp or step-like change between neighbouring patches is indicative of crystal growth, whereas according to Tomiya and Takahashi (2005) a more gradual change between neighbouring crystals will be indicative of diffusional re-equilibration.

In clinopyroxenes with patchy zoning, it can be difficult to establish whether the system processes involved are magma mixing or contamination with solid crystal debris (Streck, 2008). Tomiya and Takahashi (2005) state that intra-crystal diffusional processes (given enough time) can produce patchy zoning of the step-like variety from continuous growth bands or homogenous core areas. Streck (2008) suggests that patchy zoning can be formed from originally non-zoned crystals by melt-crystal re-equilibration processes, with these re-equilibration processes occurring along the margins of magmatic reservoirs where liquid interacts with crystal along channels and cracks, or where liquids are not in equilibrium with single suspended crystals. Streck (2008) does however state that there are no evidence of cases where patchy zoning was the result of infilling of newly crystallised pyroxene into a skeletal framework clinopyroxene crystal.

The Marion samples (especially in the backscatter and Cameca images) very closely match the physical parameters for patchy zoning. They do also show varieties of patchy zoning, with step-like sharp boundaries visible on the Cameca and the backscatter images, as well as the more gradual boundaries which could be interpreted as possibly relating to diffusion processes. It is this possible that the zoning is created by a mixture of processes, rather than a single dominant process.

### *4.2 Chemistry of the Marion clinopyroxene megacrysts*

Though the zoning in the Marion megacrysts is complex, the chemistry of the different domains still reflects the chemistry and conditions within the magma chamber under Marion Island where these crystals formed. For the Marion crystals, several compositional grouping can be discerned in the chemical data. The $Cr_2O_3$ vs. $TiO_2$ vs. $Al_2O_3$ diagram (Figure 24) can clearly be divided into three groupings; this in conjunction with Figure 22 and 23, which also can be subdivided into three groups and the Cameca images, all point to three stages of growth during crystallization of the liquid. According to Krause *et al.,* (2007) more primitive magma would contain higher concentrations of $Cr_2O_3$ and lower concentrations of $TiO_2$. As the liquid starts to crystallise, the Cr in the liquid will be incorporated into the crystal structure and, relative to the $Cr_2O_3$ concentration of the liquid, the $TiO_2$ concentration will increase. The majority of the microprobe results plot in the lower $Cr_2O_3$ and higher $TiO_2$ range, thus implying that the majority of the crystal growth occurred in a slightly more evolved liquid rather than a purely primitive mantle melt. Figures 16, 17 & 20 also reveal three different zones. In Figure 20 the lightest shade of grey would indicate the part of the crystal that was crystallised from the most primitive liquid and the darkest shading would be the part of the crystal crystallised from the most evolved liquid.

Based on a model by Aydin *et al.* (2009), the microprobe analysis can be used to get estimate on the pressure conditions under which the crystallisation of the clinopyroxene crystals occurred. Fig 25 illustrates that crystallisation occurred at some point at between 5 – 10 or 20 kbar, which correlates to between 15 – 60 km depth. However using the much more advanced Nimis and Taylor (2000) single clinopyroxene geobarometer (Fig 26), modelled at 1200K, produced a possible crystallisation pressure range of between 9 and 21 kbar (which correlates up to depths of 60km's). The distribution also roughly groups into three groups which correlate with the grouping seen in the microprobe maps (Fig 14 -20) and the triangle plots (Fig 22 -24). This is good evidence that the Marion crystals have their source in the magma chamber below Marion Island and partially from even deeper in the mantle, rather than forming as skeletal crystals during rapid ascent of magma from the chamber. The consistency of the depth estimate for all three compositional groupings lends weight to this conclusion. The grouping also shows that crystallisation occurred at different levels.

### *4.3. Growth of the Marion clinopyroxene megacrysts*

The growth of very large crystals from magmatic liquids is generally thought to be related to supersaturation of the crystal building components within the melt, where the supersaturation condition is created by through the rapid establishment of phase disequilibrium in the magma chamber, forcing extremely rapid crystal growth to rectify the imbalance. However, the mechanisms needed to create such disequilibrium are often controversial. The growth of the extremely large clinopyroxenes found in the scoria cones on Marion Island must be considered a consequence of both eruption processes and processes within the magma chamber. The largest proportion of the geochemical analyses made of the Marion crystals plot in the groups considered to represent less primitive magma (e.g. in Figure 23), which could also indicate that the crystal was reabsorbed or underwent melting while inside the magma chamber. A process such as this implies that at some point the liquidus of the crystallising system

was raised, and crystals already existing in the magma chamber became unstable relative to the new thermodynamic conditions. The liquidus can be raised by an increase in temperature (which may be the result of new magma influx), or compositional change in the liquid (again maybe due to a magma influx of some sort), or a change in pressure (which can easily be explained by means of the transform fault directly underneath the island, or through the eruption of the magma chamber). If this were the case it would account for the irregular patchy type zoning that is seen in the crystals.

The size of the crystals, however, would suggest either extremely long residence time in the magma chamber (fastest experimental estimate is $5 \times 10^{-9}$ cm/s) from Nakagawa *et al.,* (2002) or rapid crystal growth in a super-saturated environment (Brugger and Hammer, 2010). Long residence time would favour the achievement of equilibrium and would likely create homogeneous or regularly zoned crystals. Brugger and Hammer (2010) also suggested that the ascent process of magma may be recorded in the crystal texture. The irregular zoning pattern observed in the crystals is very erratic and random with some edges being diffuse while others showing a strong step-like characteristic (Figures 14 & 21). According to Brugger and Hammer's (2010) experiments, the creation dominantly faceted/euhedral crystals are also an indicator of a continuous decompression of the magma, whereas a multi-step decompression would result in skeletal crystals.

In order for supersaturation to be plausible, the liquidus would need to drop drastically over a short time, thus require a significant mechanism. The liquid will also have to be volatile-rich during eruption (all the clinopyroxene phenocryst are hosted in scoria), and this would suggest a rapid degassing trigger at the time of eruption.

Since extremely large clinopyroxenes have not regularly been reported from other ocean islands similar to Marion Island, there is a case to be made that

something is different about volcanism on Marion Island. In particular, the megacrysts need a volatile-rich evolved basaltic liquid, and require the occurrence of large degassing events. The suggested trigger for a large degassing event could be provided by the transform fault on which the island is situated, associated with the relatively close mid oceanic ridge. Though volcanic activity is not strongly correlated with far-field earthquakes (Manga and Brodsky, 2006), the unique tectonic location of Marion Island means that seismic activity along the transform fault may reasonably be quoted as affecting the magma chamber dynamics. Activity in this fault could easily change the pressure conditions of the magma chamber and by so doing induce an environment ideal for degassing of the liquid and lowering of the liquidus which in turn could induce supersaturation. This would not only create the conditions for rapid growth of large megacrysts, but would also create conditions in which instabilities in the magma chamber would allow for the creation of patchy zoning as seen in the crystals.

# Conclusions

The aim of this study was to determine whether or not the clinopyroxene megacrysts from Marion Island contained any significant domains or zones and if so, whether they reflect a residence history for the Marion magma chamber. Preliminary EDS results revealed that zones or domains might be present in the clinopyroxene crystals. EMPA and EMPA-mapping coupled with a finely tweaked Centaurus backscatter detector were used to image these domains or zones. Classifying the zoning or domains proved difficult as they failed to fall neatly into most of the standard classification regimes for most zoning types. However the zoning in the crystal closely represent an irregular form of patchy zoning (as can be seen in the backscatter image as well as the Cameca images), with sharp step-like boundaries and then some more gradual boundaries, which could be related to diffusion processes. Thus the crystals seem to have formed through a mixture of processes rather than a single dominant process.

Chemically the crystal domains or zoning can be grouped into three group, with the first group being the most primitive as well as the least represented. The following two groups are slightly more evolved but are also the most dominant, which implies that the majority of the crystal growth occurred at a slightly more evolved liquid rather than a purely primitive liquid. Clinopyroxene chemistry, plotted against the Aydin *et al.* (2009) model, suggests that the crystals formed between 5-10 kbar, which corresponds to a 15- 30 km depth, however the result was ambiguous at best. Modelling the data to the Nimis and Taylor (2000) model at a temperature of 1200K, suggested that the crystals formed at a pressure of 9 – 21 kbar. These pressure estimates indicate that the crystals have their origin in the mantle and magma chamber below the island.

Supersaturation of the liquid in the chamber is thought to be the most plausible explanation for the megacrystic size of the crystals. Various triggers have been suggested for the disequilibrium of the liquid leading to the rapid growth of the crystals, such as the influx of hot magma to raise the liquidus, or significantly change the composition of the liquid, or even by means of reactivation of the transform fault directly underneath the island to rapidly and significantly change the pressure conditions of the liquid. A long residence time is considered implausible as such a long crystal time would favour the achievement of equilibrium, which would lead to homogenous crystals rather than the complex zoning we observe in the crystals.

For supersaturation to be plausible the liquidus would change to drop significantly over a short period of time. For this a drastic mechanism is required. For scoria to form there would also need to be a significant volatile presence in the magma with a rapid degassing trigger. Very few similar cases of clinopyroxene megacryst formation (of this extend) have been reported from similar settings, thus implying a unique or rare circumstance for the Marion volcano.

It is believed that a volatile rich evolved basaltic liquid and the presence of a large degassing event is needed for these extremely large megacrysts to form. In this case the transform fault below Marion Island could provide mobilisation along the fault would provide the necessary trigger for the degassing of the liquid, leading to a liquid supersaturated with respect to clinopyroxene. Another trigger could be the massive land slide on the southern side of the island (adjacent to Pyroxene Hill). A possible combination of the two could give a significant enough trigger for the degassing of the liquid. Thereafter rapid growth of large crystals, followed by imperfect diffusion and creation of patchy zoning, resulted in the formation of the Marion Island megacrysts found in the scoria cones at surface.

## References

Aydim, F., Karsli, O., Sadiklar, M.B., (2009) Compositional Variations, Zoning Types and Petrogenetic Implications of Low-pressure Clinopyroxenes in the Neogene Alkaline Volcanic Rocks of Northeastern Turkey. *Turkish Journal of Earth Sciences*, **18**, 163-186

Boelhouwers, J.C., Meiklejohn, K.I., Holness, S.D., Hedding, D.W. Chapter 4 In *Chown, S.L. (eds.), Froneman, P.W. (eds) (2008).* The Prince Edward Islands, Land-Sea Interactions in a changing Ecosystem. Sun Press, Stellenbosch. pp 65-67

Brugger, C.R., Hammer, J., (2010). Crystallization Kinetics in Continuous Decompression Experiments: Implications for Interpreting Natural Magma Ascent Processes. *Journal Of Petrology*, **51** (9), 1941-1965

Chevallier, L. (1986). Tectonics of Marion and Prince Edward Volcanoes (Indian Ocean): Result of regional control and edifice dynamics. *Tectonophysics*, **124**, 155-175

Deer, W.A., Howie, R.A., Zussman., (1992) *An introduction to The Rock Forming Minerals* (2nd ed.). Longman, London, pp 143-154

Dowty, E., (1976). Crystal structure and crystal growth: II. Sector zoning in minerals. *American Mineralogist*, **61**, 460-469

Google Earth® (accessed on the 25th of October 2009)

Hollister, L.S., Gancarz, A.J., (1971). Compositional sector-zoning in clinopyroxene from the Narce area, Italy. *The American Mineralogist*, **56**, 959-979

Hollister, L.S., (1996). Origin, mechanism, and consequences of compositional sector-zoning in staurolite. *The American Mineralogist*, **55**, 742-766

Holten, T., Jamtveit, B., Meakin, P., Cortini, M., Blundy, J., Austrheim, H., (1997). Statistical characteristics and origin of oscillatory zoning in crystals. *The American Mineralogist*, **82**, 596-606

Krause, J., Brügmann, G.E., Pushkarev, E.V., (2007). Accessory and rock forming minerals monitoring the evolution of zoned mafic-ultramafic complexes in the central Ural mountains. *Lithos*, **95**, 19-42

LeMasurier, W.E., Thompson, J.W., (1990) Antarctic Research Series, Volume 48 Volcanoes of the Antarctic Plate and Southern Oceans. American Geophysical Union, Washington, D.C. pp 411-419

le Roux, A.P., Chevallier, L., Verwoerd, W.J., Barends, R., (2012). Petrology and geochemistry of Marion and Prince Edward Island, Southern Ocean: Magma chamber process and source region characteristics. *Journal of Volcanology and Geothermal Research,* **223-224**, 11-28

Manga, M., Brodsky, E., (2006). Seismic triggering of eruptions in the far field: Volcanoes and Geysers. *Annual Review of Earth and Planetary Sciences*, **34**, 263-291

McBirney, A.R., (2007) *Igneous Petrology* (3rd ed.). Sudbury, Jones & Bartlett, pp 422-424

McDougall, I., Verwoerd, W., Chevallier, L., (2001). K-Ar geochronology of Marion Island, Southern Ocean. *Geology Magazine*, **138** (1), 1-17

Morgan, D.J., Blake S., (2006). Magmatic residence times of zoned phenocrysts: introduction and application of the binary element diffusion modelling (BEDM) technique. *Contributions to Mineralogy and Petrology*, **151**, 58-70

Nakagawa, M., Wada, K., Wood, P., (2002). Mixed Magmas, Mush Chambers and Eruption Triggers: Evidence from Zoned Clinopyroxene Phenocrysts in Andesitic Scoria from the 1995 Eruptions of Ruapehu Volcano, New Zealand. *Journal of Petrology*, **43** (12), 2279-2303

Nimis, P., Taylor, W.R., (2000). Single clinopyroxene thermobarometry for garnet peridotites. Part 1. Calibration and testing of a Cr-in-Cpx barometer and an enstatite-in-Cpx thermometer. *Contributions to mineral Petrology*, **139**, 541-554

Royer, J., Sclater, J.G., Sandwell, D.T., (1989).A preliminary tectonic fabric chart of the Indian Ocean. *Journal of Earth System Science*, **98** (1), 7-24

Shore, M., Fowler, A.D., (1996). Oscillatory in minerals: a common phenomenon. *The Canadian Mineralogist*, **34**, 1111-1126

Stewart, M.L., Pearce, T.H., (2004). Sieve-textured plagioclase in dacitic magma: Interference imaging results. *American Mineralogist*, **89**, 348-351

Streck, M.J., (2008). Mineral Textures and Zoning as Evidence for Open System Processes. *Reviews in Mineralogy & Geochemistry*, **69**, 595-622

Sumner, P.D. (2004). Rock Weathering Rates on Subantarctic Marion Island. *Arctic, Antarctic, and Alpine Research*, **36** (1), 123-127

Tomiya, A., Takahashi, E., (2005). Evolution of the Magma Chamber beneath Usu Volcano since 1663: a Natural Laboratory for Observing Changing Phenocryst Compositions and Textures. *Journal of Petrology*, **46**, 2395-2426

Vance, J.A., (1965). Zoning in Igneous Plagioclase: Patchy. *The Journal of Geology*, **73** (4), pp. 636-651

Verwoerd, W.J., Geology. In *Van Zinderen Bakker, E.M., Winterbottom. J.M., Dyer, R.A.* (1971) Marion and Prince Edward Islands. Balkema, Cape Town, pp 40-62

Verwoerd, W.J., Marion Island. In *LeMasurier, W.E., Thomson, J.W.,* (1990) Volcanoes of the Antarctic Plate and southern Oceans. Washington, D.C.: American Geophysical union, Antarctic Research Series no. 48, pp 411-419k

# Appendices

## *Appendix I*

SEM analysis data as reported by analytical software.

| Spot | Cr | Ti | Fe | Ca | Mg | Na | Al | Si | O |
|---|---|---|---|---|---|---|---|---|---|
| 1 | 0.4 | 1.3 | 5.6 | 15.9 | 8.1 | 0 | 3.9 | 22.8 | 42.1 |
| 2 | 0.4 | 1.4 | 5.8 | 15.7 | 8.1 | 0.4 | 3.7 | 22.5 | 42 |
| 3 | 0.4 | 1.3 | 5.7 | 15.7 | 8.3 | 0.7 | 3.8 | 22.6 | 41.5 |
| 4 | 0 | 1.2 | 6 | 15.9 | 8.4 | 0.5 | 3.7 | 23.4 | 40.9 |
| 5 | 0.3 | 1.1 | 6 | 15.6 | 8.2 | 0.5 | 3.6 | 22.7 | 41.9 |
| 6 | 0.4 | 1.5 | 5.8 | 15.6 | 7.9 | 0 | 4 | 22.8 | 42.1 |
| 7 | 0 | 1.4 | 6 | 15.8 | 8.3 | 0.5 | 4 | 22.5 | 41.5 |
| 8 | 0.3 | 1.2 | 5.7 | 15.6 | 8.4 | 0.6 | 3.7 | 22.8 | 41.6 |
| 9 | 0.4 | 1 | 4.7 | 15.9 | 9.3 | 0.3 | 2.6 | 24.1 | 41.6 |
| 10 | 0.6 | 0.9 | 3.9 | 15.4 | 9.4 | 0.4 | 2.3 | 23.7 | 43.4 |
| 11 | 0.3 | 1.1 | 5.7 | 15.8 | 8 | 0 | 3.7 | 22.9 | 42.5 |
| 12 | 0.3 | 1.2 | 5.7 | 15.7 | 8.5 | 0.6 | 3.8 | 23 | 41.2 |
| 13 | 0 | 1.2 | 5.6 | 15.9 | 8.5 | 0.5 | 3.8 | 23.1 | 41.3 |
| 14 | 0.4 | 1.2 | 5.7 | 15.6 | 8.2 | 0.3 | 3.7 | 22.8 | 42 |
| 15 | 0.6 | 0.9 | 5 | 16 | 8.9 | 0.4 | 2.7 | 23.5 | 42 |
| 16 | 0.6 | 1 | 5 | 16 | 8.9 | 0.5 | 2.8 | 23.6 | 41.6 |
| 17 | 0.8 | 0.7 | 4.9 | 15.8 | 8.9 | 0.3 | 2.6 | 24.1 | 41.9 |
| 18 | 0.8 | 0.5 | 4.5 | 15.4 | 9.7 | 0 | 2.2 | 24.5 | 42.4 |
| 19 | 0.7 | 0.4 | 4.7 | 14.7 | 10.3 | 0.4 | 1.4 | 24.9 | 42.4 |
| 20 | 0.7 | 0.3 | 4.7 | 14 | 10.7 | 0 | 1.3 | 25.4 | 42.9 |
| 21 | 0.8 | 0 | 4.7 | 14.1 | 11.1 | 0 | 1.3 | 25.4 | 42.5 |
| 22 | 0.6 | 0.2 | 4.3 | 14.2 | 10.7 | 0 | 1.4 | 25.3 | 43.3 |
| 23 | 0.7 | 0.4 | 4.4 | 13.9 | 11.1 | 0 | 1.4 | 25.2 | 42.9 |

| Spot | Cr | Ti | Fe | Ca | Mg | Na | Al | Si | O |
|---|---|---|---|---|---|---|---|---|---|
| 24 | 0.6 | 0.4 | 4.2 | 14.2 | 10.8 | 0 | 1.4 | 25.1 | 43.3 |
| 25 | 0.7 | 0.4 | 4.6 | 14.4 | 10.6 | 0.6 | 1.6 | 24.9 | 42.4 |
| 26 | 0.6 | 0.4 | 4.4 | 14.5 | 10.3 | 0.5 | 1.7 | 24.9 | 42.7 |
| 27 | 0.7 | 0.5 | 4.7 | 15 | 10 | 0 | 1.9 | 24.9 | 42.4 |
| 28 | 0.9 | 0.6 | 4.6 | 15.2 | 10 | 0.5 | 1.9 | 24.7 | 41.6 |
| 29 | 0.5 | 0.3 | 5 | 14.4 | 10.7 | 0.6 | 1.3 | 25.1 | 42.1 |
| 30 | 0.9 | 0.4 | 4.3 | 14.7 | 10.1 | 0 | 1.6 | 24.9 | 43.1 |
| 31 | 0.8 | 0.2 | 4.6 | 14.9 | 10.3 | 0.3 | 1.5 | 25 | 42.4 |
| 32 | 0.6 | 0.5 | 4.9 | 15.3 | 9.7 | 0 | 2.1 | 24.9 | 42 |
| 33 | 0.7 | 0.7 | 4.6 | 15.6 | 9.3 | 0 | 2.4 | 24.1 | 42.7 |
| 34 | 0.6 | 0.6 | 5.1 | 15.4 | 9.3 | 0 | 2.6 | 24.3 | 42.2 |
| 35 | 0.6 | 0.6 | 5 | 15.4 | 9.8 | 0 | 2.1 | 24.6 | 41.9 |
| 36 | 0.7 | 0.5 | 4.9 | 15.1 | 9.7 | 0 | 1.9 | 24.7 | 42.5 |
| 37 | 0.5 | 0.8 | 4.9 | 15.6 | 9.5 | 0.6 | 2.2 | 24 | 41.9 |
| 38 | 0.5 | 0.7 | 4.7 | 15.7 | 9.2 | 0.6 | 2.6 | 24.3 | 41.6 |
| 39 | 0.6 | 0.6 | 4.9 | 15.8 | 9.6 | 0.4 | 2.4 | 24.6 | 41.2 |
| 40 | 0.5 | 0.6 | 5.1 | 15.2 | 9.5 | 0.5 | 2.3 | 24.2 | 42.1 |
| 41 | 0.6 | 0.5 | 5 | 15.6 | 9.4 | 0.3 | 2.3 | 24.3 | 41.9 |
| 42 | 0.6 | 0.7 | 4.9 | 15.8 | 9 | 0 | 2.5 | 23.8 | 42.7 |
| 43 | 0.6 | 0.7 | 4.9 | 15.7 | 9.1 | 0.3 | 2.5 | 24.1 | 42.2 |
| 44 | 0.4 | 0.7 | 4.8 | 15 | 10.2 | 0 | 1.3 | 25.5 | 42.2 |
| 45 | 0.6 | 0.6 | 5 | 15.8 | 9 | 0 | 2.7 | 23.8 | 42.4 |
| 46 | 0.6 | 0.8 | 4.5 | 15.7 | 9.2 | 0.3 | 2.5 | 23.8 | 42.6 |
| 47 | 0.6 | 0.8 | 4.7 | 15.5 | 9.5 | 0.3 | 2.5 | 24.3 | 41.9 |
| 48 | 0.6 | 0.7 | 4.7 | 15.4 | 9.4 | 0.5 | 2.4 | 24.2 | 42 |
| 49 | 0.6 | 0.6 | 4.9 | 15.2 | 9.5 | 0.3 | 2.3 | 24.2 | 42.2 |
| 50 | 0.6 | 0.5 | 5 | 15.5 | 9.7 | 0 | 2.4 | 24.2 | 42.1 |
| 51 | 0.7 | 0.3 | 4.5 | 15 | 10.1 | 0 | 1.6 | 24.9 | 42.9 |

| Spot | Cr | Ti | Fe | Ca | Mg | Na | Al | Si | O |
|---|---|---|---|---|---|---|---|---|---|
| 52 | 0.7 | 0.5 | 4.8 | 14.4 | 10.4 | 0.6 | 1.8 | 24.8 | 42 |
| 53 | 0.6 | 0.4 | 4.6 | 14.2 | 10.4 | 0.3 | 1.6 | 25 | 42.9 |
| 54 | 0.6 | 0.6 | 4.7 | 14.7 | 10 | 0.5 | 2.1 | 24.7 | 42.1 |
| 55 | 0.5 | 0.5 | 4.8 | 14.4 | 10.3 | 0 | 1.8 | 24.8 | 42.9 |
| 56 | 0.6 | 0.5 | 4.9 | 14.6 | 10.2 | 0.3 | 1.9 | 24.6 | 42.4 |
| 57 | 0.6 | 0.5 | 5.1 | 14.7 | 10.1 | 0 | 2.1 | 24.4 | 42.5 |
| 58 | 0.5 | 0.5 | 4.7 | 14.7 | 9.8 | 0.5 | 2.1 | 24.4 | 42.9 |
| 59 | 0.5 | 0.6 | 4.9 | 14.9 | 9.7 | 0.4 | 2.1 | 24.5 | 42.4 |
| 60 | 0.6 | 0.6 | 4.8 | 14.8 | 10.2 | 0.5 | 1.8 | 24.7 | 42 |
| 61 | 0.7 | 0.5 | 4.7 | 15 | 10.2 | 0.7 | 1.7 | 24.8 | 41.7 |
| 62 | 0.6 | 0.5 | 5.1 | 15 | 10.1 | 0.6 | 1.8 | 24.5 | 41.7 |
| 63 | 0.5 | 0.6 | 5.2 | 15.2 | 9.6 | 0 | 2.2 | 24.3 | 42.3 |
| 64 | 0.6 | 0.6 | 5.2 | 15.1 | 9.6 | 0.4 | 2.4 | 24.2 | 41.9 |
| 65 | 0.5 | 0.8 | 5.1 | 15 | 9.7 | 0.5 | 2.3 | 24.1 | 42 |
| 66 | 0.7 | 0.6 | 5.3 | 14.8 | 9.3 | 0 | 2.5 | 24.2 | 42.6 |
| 67 | 0.5 | 0.6 | 5.1 | 14.6 | 9.5 | 0.6 | 2.6 | 24.1 | 42.4 |
| 68 | 0.5 | 0.6 | 5.1 | 15 | 9.4 | 0 | 2.6 | 24.3 | 42.5 |
| 69 | 0.5 | 0.7 | 5.2 | 15.1 | 9.5 | 0.5 | 2.4 | 24.2 | 41.9 |
| 70 | 0.6 | 0.8 | 4.9 | 15.3 | 9.3 | 0 | 2.6 | 23.9 | 42.7 |
| 71 | 0.6 | 0.6 | 5 | 15.6 | 9.1 | 0 | 2.6 | 24 | 42.5 |
| 72 | 0.5 | 0.6 | 5 | 15.7 | 9.2 | 0.3 | 2.5 | 23.8 | 42.3 |
| 73 | 0.6 | 0.8 | 5 | 15.6 | 9.4 | 0.3 | 2.6 | 24.1 | 41.6 |
| 74 | 0.5 | 0.7 | 4.6 | 15.8 | 9.3 | 0.4 | 2.6 | 24.2 | 41.9 |
| 75 | 0.6 | 0.7 | 4.8 | 15.4 | 9.4 | 0.6 | 2.3 | 24.3 | 42 |
| 76 | 0.6 | 0.6 | 4.6 | 15.7 | 9.1 | 0 | 2.5 | 24.2 | 42.7 |
| 77 | 0.7 | 0.7 | 4.6 | 15.8 | 9.2 | 0 | 2.2 | 24.1 | 42.8 |
| 78 | 0.7 | 0.8 | 4.6 | 15.2 | 9.3 | 0 | 2.1 | 24.3 | 42.9 |
| 79 | 0.6 | 0.5 | 4.7 | 15 | 9.7 | 0.3 | 1.9 | 24.4 | 42.9 |

| Spot | Cr | Ti | Fe | Ca | Mg | Na | Al | Si | O |
|---|---|---|---|---|---|---|---|---|---|
| 80 | 0.6 | 0.5 | 5.1 | 15 | 9.8 | 0.6 | 2.2 | 24.3 | 42 |
| 81 | 0.6 | 0.7 | 5.3 | 14.6 | 9.9 | 0.3 | 1.9 | 24.5 | 42.3 |
| 82 | 0.7 | 0.4 | 4.7 | 14.6 | 10 | 0.3 | 1.7 | 24.9 | 42.6 |
| 83 | 0.6 | 0.5 | 4.8 | 14.8 | 10.3 | 0.3 | 1.7 | 24.8 | 42.1 |
| 84 | 0.5 | 0.4 | 4.8 | 14.8 | 10.3 | 0.3 | 1.7 | 24.6 | 42.6 |
| 85 | 0.7 | 0.5 | 4.7 | 14.5 | 9.9 | 0 | 2.1 | 24.5 | 43.1 |
| 86 | 0.7 | 0.6 | 4.9 | 14.6 | 10.1 | 0.6 | 2.2 | 24.4 | 41.9 |
| 87 | 0.6 | 0.7 | 5.1 | 14.3 | 10 | 0.3 | 2.2 | 24.5 | 42.2 |
| 88 | 0.6 | 0.6 | 5 | 14.7 | 10.1 | 0.3 | 1.6 | 24.7 | 42.4 |
| 89 | 0.6 | 0.4 | 4.7 | 14.6 | 10.3 | 0 | 1.7 | 24.8 | 42.8 |
| 90 | 0.7 | 0.7 | 4.4 | 15.1 | 9.6 | 0 | 2.2 | 24.5 | 42.7 |
| 91 | 0.5 | 0.6 | 5 | 15.1 | 9.7 | 0.3 | 2.1 | 24.5 | 42.1 |
| 92 | 0.7 | 0.5 | 4.8 | 15.2 | 9.7 | 0.3 | 2.3 | 24.4 | 42.1 |
| 93 | 0.6 | 0.7 | 4.8 | 15.2 | 9.6 | 0 | 2.2 | 24.4 | 42.5 |
| 94 | 0.6 | 0.6 | 5 | 15.4 | 9.3 | 0 | 2.3 | 24.1 | 42.6 |
| 95 | 0.7 | 0.6 | 4.8 | 15.9 | 9.4 | 0.3 | 2.3 | 24.4 | 41.6 |
| 96 | 0.5 | 0.5 | 4.3 | 14 | 9.5 | 0.3 | 2.1 | 23.5 | 45.1 |
| 97 | 0.5 | 0.5 | 4.7 | 15.4 | 9.5 | 0 | 2.4 | 24.1 | 24.7 |
| 98 | 0.5 | 0.7 | 4.8 | 15.5 | 9.4 | 0 | 2.3 | 24.3 | 42.5 |
| 99 | 0.7 | 0.6 | 4.7 | 15 | 9.6 | 0.3 | 2.1 | 24.4 | 42.6 |
| 100 | 0.6 | 0.5 | 4.7 | 15.3 | 9.7 | 0.3 | 2 | 24.4 | 42.5 |
| 101 | 0.7 | 0.7 | 5.1 | 15.3 | 9.3 | 0 | 2.2 | 24.3 | 42.4 |
| 102 | 0.7 | 0.6 | 4.8 | 15.2 | 9.5 | 0 | 2.3 | 24.4 | 42.5 |
| 103 | 0.6 | 0.5 | 4.5 | 15.1 | 9.9 | 0.4 | 2.2 | 24.4 | 42.5 |
| 104 | 0.7 | 0.6 | 4.9 | 14.7 | 9.8 | 0 | 1.8 | 24.9 | 42.7 |
| 105 | 0.6 | 0.6 | 4.6 | 14.2 | 10.1 | 0.3 | 19 | 24.5 | 43.4 |
| 106 | 0.6 | 0.4 | 4.4 | 14.8 | 10.1 | 0 | 1.8 | 25.1 | 42.8 |
| 107 | 0.7 | 0.5 | 4.4 | 14.8 | 10.1 | 0.4 | 1.8 | 24.7 | 42.8 |

| Spot | Cr | Ti | Fe | Ca | Mg | Na | Al | Si | O |
|---|---|---|---|---|---|---|---|---|---|
| 108 | 0.7 | 0.6 | 4.5 | 14.8 | 10.1 | 0 | 2 | 24.8 | 42.6 |
| 109 | 0.5 | 0.7 | 5.1 | 14.3 | 10 | 0.4 | 2.2 | 24.4 | 42.2 |
| 110 | 0.6 | 0.6 | 4.5 | 14 | 10.1 | 0 | 1.8 | 24.4 | 44.1 |
| 111 | 0.7 | 0.4 | 4.3 | 14.5 | 10.5 | 0 | 1.5 | 25 | 43.1 |
| 112 | 0.7 | 0.4 | 4.4 | 14.4 | 10.3 | 0 | 1.5 | 25.1 | 43.2 |
| 113 | 0.6 | 0.5 | 4.6 | 14.6 | 10.3 | 0.3 | 1.7 | 24.8 | 42.6 |
| 114 | 0.6 | 0.6 | 4.8 | 14.6 | 10.1 | 0 | 2 | 24.6 | 42.7 |
| 116 | 0.8 | 0.3 | 4.4 | 14.4 | 10.5 | 0 | 1.6 | 24.8 | 43.1 |
| 117 | 0.8 | 0 | 4.8 | 14.2 | 10.9 | 0.5 | 1.2 | 25.3 | 41.7 |
| 118 | 0.8 | 0.4 | 4.6 | 14.3 | 10.5 | 0.3 | 1.5 | 25 | 42.8 |
| 119 | 0.6 | 0.2 | 4.7 | 14.6 | 10.5 | 0 | 1.5 | 25.3 | 42.6 |
| 120 | 0.8 | 0.3 | 4.3 | 14.3 | 10.4 | 0 | 1.5 | 25 | 43.3 |
| 121 | 0.8 | 0.5 | 4.4 | 14.8 | 10.2 | 0.2 | 2 | 24.7 | 42.5 |
| 122 | 0.8 | 0.3 | 4.4 | 14.2 | 10.8 | 0.4 | 1.4 | 25.2 | 42.5 |
| 123 | 0.8 | 0.3 | 4.5 | 14.1 | 10.8 | 0 | 1.4 | 25.3 | 42.9 |
| 124 | 0.7 | 0.4 | 4.3 | 14.3 | 10.7 | 0 | 1.4 | 25.1 | 43.1 |
| 125 | 0.8 | 0.6 | 4.4 | 14.5 | 10.1 | 0.3 | 2.1 | 24.6 | 42.6 |
| 126 | 0.6 | 0.6 | 4.7 | 14.4 | 9.9 | 0 | 2.1 | 24.4 | 43.3 |
| 127 | 0.8 | 0.5 | 4.8 | 15.2 | 9.5 | 0 | 2.2 | 24.6 | 42.5 |
| 128 | 0.6 | 0.6 | 4.8 | 15.2 | 9.4 | 0.5 | 2.4 | 24.2 | 42.2 |
| 129 | 0.7 | 0.6 | 4.9 | 15.2 | 9.6 | 0.3 | 2.3 | 24.4 | 42 |
| 130 | 0.6 | 0.7 | 4.9 | 14.8 | 9.5 | 0 | 2.1 | 24.4 | 42.9 |
| 131 | 0.5 | 0.5 | 5.1 | 15 | 9.6 | 0 | 2 | 24.7 | 42.7 |
| 132 | 0.5 | 0.5 | 5.1 | 15.1 | 9.7 | 0 | 2 | 24.5 | 42.5 |
| 133 | 0.7 | 0.5 | 5 | 15.2 | 9.9 | 0.5 | 2 | 24.6 | 41.5 |
| 134 | 0.7 | 0.4 | 5.2 | 14.9 | 10.1 | 0.5 | 2.3 | 24.8 | 41 |
| 135 | 0.7 | 0.5 | 4.7 | 14.8 | 9.9 | 0.6 | 2.1 | 24.3 | 42.5 |
| 136 | 0.5 | 0.7 | 4.7 | 15 | 9.5 | 0 | 2.4 | 24.4 | 42.6 |

| Spot | Cr | Ti | Fe | Ca | Mg | Na | Al | Si | O |
|---|---|---|---|---|---|---|---|---|---|
| 137 | 0.5 | 0.6 | 4.8 | 15.1 | 9.4 | 0 | 2.2 | 24.6 | 42.7 |
| 138 | 0.6 | 0.5 | 4.6 | 15.4 | 9.6 | 0.5 | 2.2 | 24.1 | 42.6 |
| 139 | 0.5 | 0.8 | 4.9 | 15.1 | 9.3 | 0 | 2.4 | 24.4 | 42.6 |
| 140 | 0.6 | 0.6 | 4.6 | 15.3 | 9.4 | 0 | 2.4 | 24.2 | 42.9 |
| 141 | 0.6 | 0.6 | 5 | 15.1 | 9.6 | 0.4 | 2.3 | 24.2 | 42.2 |
| 142 | 0.6 | 0.6 | 4.6 | 14.9 | 9.7 | 0 | 2.2 | 24.5 | 42.8 |
| 143 | 0.6 | 0.6 | 4.9 | 15.2 | 9.4 | 0 | 2.2 | 24.4 | 42.8 |

*Appendix II*

Large interval microprobe data as reported by analytical software.

| Sample 2 | $SiO_2$ | $TiO_2$ | $Al_2O3$ | $Cr_2O_3$ | FeO | MnO | MgO | CaO | $Na_2O$ |
|---|---|---|---|---|---|---|---|---|---|
| 5 / 1 . | 48.37 | 1.84 | 7.41 | 0.43 | 6.92 | 0.09 | 13.86 | 20.93 | 0.51 |
| 5 / 2 . | 50.19 | 1.25 | 5.29 | 0.56 | 5.85 | 0.11 | 15.21 | 21.61 | 0.4 |
| 5 / 3 . | 50.46 | 1.23 | 5.35 | 0.58 | 6.01 | 0.12 | 15.32 | 21.5 | 0.36 |
| 5 / 4 . | 49.29 | 1.52 | 6.37 | 0.7 | 6.55 | 0.09 | 14.55 | 20.76 | 0.51 |
| 5 / 5 . | 50.71 | 1.12 | 5.19 | 0.67 | 5.76 | 0.11 | 15.31 | 21.62 | 0.38 |
| 5 / 6 . | 50.64 | 1.16 | 5.44 | 0.66 | 5.86 | 0.14 | 15.27 | 21.44 | 0.4 |
| 5 / 7 . | 50.44 | 1.15 | 5.14 | 0.72 | 5.71 | 0.11 | 15.27 | 21.67 | 0.38 |
| 5 / 8 . | 49.41 | 1.64 | 6.8 | 0.44 | 6.69 | 0.11 | 14.59 | 21.03 | 0.49 |
| 5 / 9 . | 49.63 | 1.52 | 6.1 | 0.53 | 6.24 | 0.1 | 14.74 | 21.45 | 0.43 |
| 5 / 10 . | 50.47 | 1.25 | 5.34 | 0.52 | 5.81 | 0.07 | 15.09 | 21.78 | 0.38 |
| 5 / 11 . | 49.59 | 1.54 | 6.35 | 0.52 | 6.33 | 0.13 | 14.84 | 21.29 | 0.47 |
| 5 / 12 . | 50.66 | 1.14 | 5.38 | 0.58 | 6.1 | 0.13 | 15.41 | 21.56 | 0.41 |
| 5 / 13 . | 48.75 | 1.74 | 7.27 | 0.48 | 6.93 | 0.12 | 14.09 | 20.81 | 0.51 |
| 5 / 14 . | 49.06 | 1.7 | 7.05 | 0.46 | 6.87 | 0.13 | 14.22 | 21.15 | 0.5 |
| 5 / 15 . | 50.72 | 1.07 | 5.33 | 0.53 | 5.9 | 0.12 | 15.45 | 21.21 | 0.38 |
| 5 / 16 . | 50.55 | 1.11 | 5.32 | 0.64 | 5.87 | 0.08 | 15.23 | 21.23 | 0.4 |
| 5 / 17 . | 50.61 | 1.29 | 5.5 | 0.51 | 6.07 | 0.11 | 15.31 | 21.24 | 0.41 |
| 5 / 18 . | 50.3 | 1.15 | 5.36 | 0.69 | 5.84 | 0.09 | 15.15 | 21.38 | 0.4 |
| 5 / 19 . | 48.91 | 1.72 | 6.81 | 0.52 | 6.88 | 0.13 | 14.18 | 21.12 | 0.52 |
| 5 / 20 . | 50.21 | 1.2 | 5.39 | 0.69 | 5.77 | 0.1 | 15.24 | 21.69 | 0.39 |
| 5 / 21 . | 50.16 | 1.2 | 5.33 | 0.67 | 6.02 | 0.11 | 15.2 | 21.32 | 0.42 |
| 5 / 22 . | 50.58 | 1.14 | 5.23 | 0.66 | 5.98 | 0.08 | 15.28 | 21.55 | 0.38 |
| 5 / 23 . | 51.57 | 1.09 | 4.92 | 0.42 | 6.09 | 0.11 | 15.64 | 21.53 | 0.4 |
| 5 / 24 . | 48.89 | 1.64 | 6.55 | 0.58 | 6.99 | 0.13 | 14.3 | 21.2 | 0.49 |
| 5 / 25 . | 50.45 | 1.13 | 5.15 | 0.68 | 5.91 | 0.13 | 15.1 | 21.53 | 0.39 |
| 5 / 26 . | 50.15 | 1.16 | 4.9 | 0.7 | 5.8 | 0.09 | 15.36 | 21.67 | 0.38 |
| 5 / 27 . | 48.79 | 1.63 | 6.79 | 0.53 | 6.66 | 0.07 | 14.38 | 21.27 | 0.48 |
| 5 / 28 . | 50.04 | 1.07 | 4.81 | 0.68 | 5.89 | 0.08 | 15.04 | 21.56 | 0.36 |
| 5 / 29 . | 49.38 | 1.09 | 4.91 | 0.64 | 5.92 | 0.11 | 15.17 | 21.29 | 0.39 |
| 5 / 30 . | 47.84 | 1.58 | 6.49 | 0.46 | 6.25 | 0.08 | 13.94 | 21.69 | 0.42 |

| Sample 4 | $SiO_2$ | $TiO_3$ | $Al_2O_4$ | $Cr_2O_4$ | FeO | MnO | MgO | CaO | $Na_2O$ |
|---|---|---|---|---|---|---|---|---|---|
| 1 / 1 . | 48.32 | 1.77 | 7.13 | 0.47 | 6.58 | 0.1 | 13.76 | 21.74 | 0.46 |
| 1 / 2 . | 48.35 | 1.79 | 7.1 | 0.52 | 6.63 | 0.11 | 13.77 | 21.19 | 0.46 |
| 1 / 4 . | 50.26 | 1.19 | 5.44 | 0.54 | 5.97 | 0.12 | 15.14 | 21.56 | 0.38 |
| 1 / 5 . | 49.51 | 1.44 | 6.43 | 0.45 | 6.3 | 0.14 | 14.5 | 21.32 | 0.41 |
| 1 / 6 . | 50.41 | 1.17 | 5.1 | 0.63 | 5.83 | 0.14 | 15.03 | 21.62 | 0.37 |
| 1 / 7 . | 48.43 | 1.69 | 7.02 | 0.56 | 6.61 | 0.11 | 14.12 | 21.34 | 0.47 |
| 1 / 8 . | 48.29 | 1.77 | 7.22 | 0.53 | 6.54 | 0.15 | 13.99 | 20.94 | 0.48 |
| 1 / 9 . | 48.3 | 1.77 | 7.15 | 0.47 | 6.6 | 0.14 | 14.13 | 21.26 | 0.48 |
| 1 / 10 . | 48.43 | 1.76 | 7.06 | 0.51 | 6.58 | 0.1 | 14.06 | 21.11 | 0.47 |
| 1 / 12 . | 48.6 | 1.77 | 6.95 | 0.5 | 6.56 | 0.13 | 14.27 | 21.14 | 0.48 |
| 1 / 13 . | 49.55 | 1.32 | 5.9 | 0.48 | 6.5 | 0.15 | 14.75 | 20.91 | 0.47 |
| 1 / 14 . | 48.41 | 1.75 | 7.23 | 0.46 | 6.7 | 0.1 | 14.12 | 20.86 | 0.47 |
| 1 / 15 . | 47.89 | 1.92 | 7.5 | 0.51 | 7.11 | 0.15 | 13.8 | 20.97 | 0.5 |
| 1 / 16 . | 48.3 | 1.79 | 7.27 | 0.53 | 6.77 | 0.13 | 14.07 | 21.2 | 0.48 |
| 1 / 17 . | 47.92 | 1.91 | 7.47 | 0.48 | 7.02 | 0.1 | 13.52 | 21.33 | 0.49 |
| 1 / 18 . | 48.16 | 1.85 | 7.14 | 0.52 | 6.67 | 0.11 | 14.1 | 20.92 | 0.48 |
| 1 / 19 . | 49.53 | 1.42 | 6.11 | 0.56 | 6.31 | 0.12 | 14.58 | 21.47 | 0.44 |
| 1 / 20 . | 49.23 | 1.52 | 6.31 | 0.55 | 6.45 | 0.11 | 14.13 | 20.96 | 0.41 |
| 1 / 21 . | 50.23 | 1.11 | 5.35 | 0.55 | 6.21 | 0.11 | 15.16 | 20.98 | 0.4 |
| 1 / 22 . | 50.58 | 1.13 | 5.34 | 0.5 | 5.99 | 0.13 | 15.4 | 21.49 | 0.4 |
| 1 / 23 . | 49.17 | 1.5 | 6.39 | 0.51 | 6.43 | 0.13 | 14.32 | 21.47 | 0.47 |
| 1 / 24 . | 49.05 | 1.62 | 6.53 | 0.54 | 6.49 | 0.14 | 14.27 | 21.44 | 0.46 |
| 1 / 25 . | 49.53 | 1.41 | 6.19 | 0.53 | 6.21 | 0.11 | 14.54 | 21.16 | 0.44 |
| 1 / 26 . | 49.42 | 1.46 | 6.29 | 0.57 | 6.21 | 0.11 | 14.89 | 21.22 | 0.43 |
| 1 / 27 . | 48.88 | 1.67 | 6.99 | 0.48 | 6.44 | 0.11 | 14.22 | 21.41 | 0.48 |
| 1 / 28 . | 49.88 | 1.25 | 5.52 | 0.64 | 5.94 | 0.09 | 14.95 | 21.64 | 0.38 |
| 1 / 29 . | 49.64 | 1.35 | 5.99 | 0.52 | 6.13 | 0.11 | 14.95 | 21.42 | 0.42 |
| 1 / 30 . | 48.93 | 1.73 | 6.96 | 0.52 | 6.66 | 0.09 | 14.18 | 21.43 | 0.47 |

| Sample 5 | $SiO_2$ | $TiO_3$ | $Al_2O_4$ | $Cr_2O_4$ | FeO | MnO | MgO | CaO | $Na_2O$ |
|---|---|---|---|---|---|---|---|---|---|
| 2 / 1 . | 48.08 | 1.88 | 7.39 | 0.48 | 6.96 | 0.1 | 13.8 | 21.21 | 0.5 |
| 2 / 2 . | 50.29 | 1.26 | 5.25 | 0.51 | 6.02 | 0.07 | 15.38 | 20.64 | 0.43 |
| 2 / 3 . | 52.22 | 0.65 | 3.39 | 0.56 | 5.24 | 0.1 | 16.8 | 21.14 | 0.36 |
| 2 / 4 . | 50.58 | 1.04 | 4.7 | 0.57 | 5.92 | 0.1 | 15.51 | 21.34 | 0.4 |
| 2 / 5 . | 49.75 | 1.17 | 5.23 | 0.53 | 6.08 | 0.13 | 15.27 | 21.04 | 0.42 |
| 2 / 6 . | 50.22 | 0.94 | 4.63 | 0.6 | 5.58 | 0.13 | 15.72 | 21.11 | 0.37 |
| 2 / 7 . | 50.8 | 0.64 | 3.46 | 0.49 | 5.12 | 0.1 | 16.76 | 20.92 | 0.35 |
| 2 / 8 . | 50.92 | 0.59 | 3.18 | 0.66 | 5.06 | 0.08 | 17.01 | 20.73 | 0.32 |
| 2 / 9 . | 51.39 | 0.89 | 3.95 | 1.1 | 5.14 | 0.1 | 16.27 | 20.79 | 0.4 |
| 2 / 10 . | 50.53 | 1.13 | 5 | 0.63 | 5.97 | 0.11 | 15.62 | 20.97 | 0.41 |
| 2 / 11 . | 50.83 | 1.01 | 4.53 | 0.6 | 5.94 | 0.12 | 15.77 | 21.18 | 0.4 |
| 2 / 12 . | 50.42 | 1.01 | 4.94 | 0.54 | 6.08 | 0.11 | 15.4 | 21 | 0.41 |
| 2 / 13 . | 50.56 | 1.12 | 4.96 | 0.59 | 6.19 | 0.16 | 15.37 | 21.13 | 0.42 |
| 2 / 14 . | 50.1 | 1.2 | 5.29 | 0.57 | 6.46 | 0.15 | 15.17 | 20.8 | 0.46 |
| 2 / 15 . | 50.65 | 0.99 | 4.77 | 0.61 | 5.84 | 0.11 | 15.56 | 21.4 | 0.39 |
| 2 / 16 . | 51.87 | 0.87 | 3.68 | 0.64 | 5.74 | 0.09 | 16.17 | 21.12 | 0.39 |
| 2 / 17 . | 51.2 | 1 | 4.69 | 0.56 | 5.76 | 0.12 | 15.96 | 20.91 | 0.38 |
| 2 / 18 . | 51.01 | 0.88 | 4.32 | 0.66 | 5.58 | 0.12 | 16.01 | 21.2 | 0.37 |
| 2 / 19 . | 50.54 | 1.12 | 5 | 0.6 | 6.54 | 0.12 | 15.41 | 20.69 | 0.46 |
| 2 / 20 . | 52.16 | 0.64 | 3.63 | 0.9 | 5.36 | 0.08 | 16.76 | 20.93 | 0.36 |
| 2 / 21 . | 50.99 | 0.58 | 3.42 | 0.82 | 5.08 | 0.1 | 16.79 | 20.71 | 0.36 |
| 2 / 22 . | 48.86 | 1.25 | 5.58 | 0.62 | 6.35 | 0.14 | 15.13 | 20.68 | 0.46 |
| 2 / 23 . | 51.69 | 0.64 | 3.57 | 0.84 | 5.52 | 0.14 | 16.67 | 20.62 | 0.37 |
| 2 / 24 . | 52.16 | 0.58 | 3.42 | 0.7 | 5.21 | 0.09 | 17 | 20.94 | 0.34 |
| 2 / 25 . | 50.66 | 1.01 | 4.86 | 0.61 | 5.82 | 0.09 | 15.71 | 21.17 | 0.4 |
| 2 / 26 . | 50.03 | 1.28 | 5.48 | 0.58 | 6.2 | 0.08 | 15.09 | 21.14 | 0.44 |
| 2 / 27 . | 50.37 | 1.12 | 5.17 | 0.56 | 6.34 | 0.13 | 15.16 | 21.39 | 0.42 |
| 2 / 28 . | 50.97 | 1.06 | 4.41 | 0.6 | 5.59 | 0.1 | 15.86 | 21.21 | 0.37 |
| 2 / 29 . | 51.62 | 0.56 | 3.05 | 0.58 | 5.11 | 0.1 | 16.74 | 21.36 | 0.33 |
| 2 / 30 . | 47.84 | 1.45 | 5.93 | 0.57 | 6.39 | 0.12 | 14.15 | 21.47 | 0.42 |

| Sample 6 | $SiO_2$ | $TiO_3$ | $Al_2O_4$ | $Cr_2O_4$ | FeO | MnO | MgO | CaO | $Na_2O$ |
|---|---|---|---|---|---|---|---|---|---|
| 4 / 1 . | 49.13 | 1.63 | 6.64 | 0.56 | 6.35 | 0.13 | 14.17 | 21.28 | 0.48 |
| 4 / 2 . | 49.48 | 1.56 | 5.89 | 0.44 | 6.31 | 0.14 | 14.55 | 21.83 | 0.4 |
| 4 / 3 . | 49.48 | 1.49 | 5.82 | 0.62 | 6.15 | 0.11 | 14.61 | 21.61 | 0.43 |
| 4 / 4 . | 50.15 | 1.57 | 5.02 | 0.77 | 5.95 | 0.08 | 15.04 | 22.22 | 0.36 |
| 4 / 5 . | 50.52 | 1.27 | 4.96 | 0.8 | 6.07 | 0.11 | 15.31 | 21.51 | 0.42 |
| 4 / 6 . | 51.17 | 0.9 | 4.52 | 0.81 | 5.63 | 0.09 | 16.22 | 21.07 | 0.4 |
| 4 / 7 . | 50.46 | 1.22 | 5.06 | 0.75 | 5.74 | 0.09 | 15.54 | 21.18 | 0.36 |
| 4 / 8 . | 50.91 | 1.08 | 4.92 | 0.78 | 5.81 | 0.11 | 15.69 | 21.27 | 0.41 |
| 4 / 9 . | 50.45 | 1.18 | 5.17 | 0.77 | 6 | 0.12 | 15.34 | 21.11 | 0.46 |
| 4 / 10 . | 51.04 | 1.02 | 4.76 | 0.84 | 5.62 | 0.13 | 15.87 | 21.11 | 0.4 |
| 4 / 11 . | 50.42 | 1.19 | 5.24 | 0.71 | 6.02 | 0.11 | 15.44 | 21.17 | 0.46 |
| 4 / 12 . | 50.15 | 1.18 | 5.31 | 0.76 | 6.04 | 0.11 | 15.36 | 21.23 | 0.44 |
| 4 / 13 . | 51.41 | 0.82 | 4.03 | 1.08 | 4.72 | 0.11 | 16.51 | 21.46 | 0.39 |
| 4 / 14 . | 51.17 | 0.81 | 4.04 | 0.9 | 5.31 | 0.09 | 16.22 | 21.37 | 0.38 |
| 4 / 15 . | 50.45 | 1.09 | 4.79 | 0.8 | 5.78 | 0.11 | 15.86 | 21.1 | 0.4 |
| 4 / 16 . | 50.8 | 0.84 | 4.2 | 1.07 | 4.78 | 0.11 | 16.21 | 21.45 | 0.38 |
| 4 / 17 . | 50.59 | 0.86 | 4.24 | 0.9 | 5.16 | 0.13 | 16.11 | 21.22 | 0.39 |
| 4 / 18 . | 50.76 | 0.95 | 4.12 | 1.06 | 4.72 | 0.09 | 16.13 | 21.62 | 0.39 |
| 4 / 19 . | 49.54 | 1.31 | 5.4 | 0.64 | 5.76 | 0.07 | 15.32 | 21.61 | 0.36 |
| 4 / 20 . | 48.82 | 1.34 | 5.49 | 0.82 | 5.56 | 0.1 | 14.99 | 21.85 | 0.36 |
| 4 / 21 . | 49.64 | 1.43 | 5.37 | 0.65 | 5.82 | 0.09 | 15.26 | 21.75 | 0.39 |
| 4 / 22 . | 48.16 | 1.82 | 5.9 | 0.5 | 6.32 | 0.1 | 14.28 | 22.26 | 0.35 |
| 4 / 23 . | 49.01 | 1.53 | 5.5 | 0.56 | 6.06 | 0.12 | 14.87 | 22.02 | 0.34 |
| 4 / 24 . | 49.66 | 1.16 | 5.36 | 0.57 | 5.91 | 0.09 | 15.25 | 21.88 | 0.36 |
| 4 / 25 . | 50.44 | 1.19 | 4.96 | 1 | 5.42 | 0.14 | 15.33 | 21.87 | 0.32 |
| 4 / 26 . | 49.8 | 1.35 | 5.37 | 0.62 | 5.96 | 0.12 | 15.11 | 21.53 | 0.3 |
| 4 / 27 . | 49.94 | 1.46 | 5.54 | 0.61 | 5.94 | 0.1 | 14.94 | 21.78 | 0.43 |
| 4 / 28 . | 49.43 | 1.7 | 5.57 | 0.6 | 6.08 | 0.1 | 14.56 | 22.13 | 0.4 |
| 4 / 29 . | 49.81 | 1.41 | 5.39 | 0.57 | 6.3 | 0.13 | 15.11 | 21.78 | 0.41 |
| 4 / 30 . | 49.03 | 1.48 | 6.47 | 0.41 | 6.24 | 0.13 | 14.57 | 21.75 | 0.42 |

| Sample 9 | $SiO_2$ | $TiO_3$ | $Al_2O_4$ | $Cr_2O_4$ | FeO | MnO | MgO | CaO | $Na_2O$ |
|---|---|---|---|---|---|---|---|---|---|
| 6 / 1 . | 48.39 | 2.07 | 7.45 | 0.34 | 6.94 | 0.13 | 13.87 | 21.41 | 0.5 |
| 6 / 2 . | 51.43 | 1.1 | 4.27 | 0.54 | 5.53 | 0.12 | 15.93 | 21.12 | 0.41 |
| 6 / 3 . | 51.85 | 1.08 | 4.14 | 0.55 | 5.71 | 0.1 | 16.26 | 20.8 | 0.43 |
| 6 / 4 . | 52.65 | 0.88 | 3.63 | 0.75 | 4.67 | 0.11 | 16.4 | 21.7 | 0.38 |
| 6 / 5 . | 52.7 | 0.84 | 3.37 | 0.53 | 4.87 | 0.1 | 16.81 | 21.24 | 0.37 |
| 6 / 7 . | 51.81 | 0.84 | 4.45 | 0.97 | 5.06 | 0.1 | 16.54 | 20.92 | 0.4 |
| 6 / 8 . | 51.52 | 0.81 | 4.53 | 0.97 | 4.99 | 0.13 | 16.38 | 20.93 | 0.41 |
| 6 / 9 . | 51.9 | 0.72 | 4.13 | 0.89 | 4.84 | 0.09 | 16.48 | 20.98 | 0.37 |
| 6 / 10 . | 52.08 | 0.76 | 3.9 | 0.81 | 4.95 | 0.11 | 16.61 | 21.31 | 0.38 |
| 6 / 11 . | 51.94 | 0.73 | 3.92 | 0.84 | 4.86 | 0.11 | 16.64 | 21.1 | 0.38 |
| 6 / 12 . | 51.68 | 0.84 | 4.16 | 0.89 | 4.8 | 0.1 | 16.64 | 21.04 | 0.38 |
| 6 / 13 . | 51.64 | 0.79 | 4.31 | 0.98 | 5 | 0.13 | 16.74 | 20.89 | 0.39 |
| 6 / 14 . | 51.61 | 0.81 | 4.19 | 0.99 | 5.03 | 0.09 | 16.69 | 20.73 | 0.38 |
| 6 / 15 . | 51.99 | 0.75 | 4.16 | 0.96 | 5.04 | 0.08 | 16.49 | 21.04 | 0.39 |
| 6 / 16 . | 51.82 | 0.83 | 4.25 | 1.02 | 4.98 | 0.07 | 16.42 | 21.14 | 0.39 |
| 6 / 17 . | 51.59 | 0.88 | 4.35 | 0.98 | 4.8 | 0.14 | 16.53 | 21.22 | 0.41 |
| 6 / 18 . | 52.1 | 0.75 | 3.99 | 0.87 | 4.99 | 0.1 | 16.64 | 21.19 | 0.38 |
| 6 / 19 . | 52 | 0.78 | 3.96 | 0.87 | 4.81 | 0.06 | 16.47 | 21.34 | 0.38 |
| 6 / 20 . | 52.1 | 0.77 | 3.91 | 0.87 | 4.96 | 0.09 | 16.57 | 21.31 | 0.39 |
| 6 / 21 . | 52.22 | 0.71 | 3.86 | 0.82 | 4.9 | 0.08 | 16.41 | 21.41 | 0.36 |
| 6 / 22 . | 52.13 | 0.82 | 4.27 | 0.98 | 4.98 | 0.1 | 16.35 | 21.29 | 0.39 |
| 6 / 23 . | 52.9 | 0.73 | 3.21 | 0.85 | 4.57 | 0.1 | 16.91 | 21.83 | 0.38 |
| 6 / 24 . | 52.56 | 0.67 | 3.36 | 0.75 | 4.83 | 0.1 | 16.84 | 21.1 | 0.37 |
| 6 / 25 . | 52.2 | 0.85 | 3.57 | 0.71 | 5.03 | 0.08 | 16.88 | 21.4 | 0.36 |
| 6 / 26 . | 53.08 | 0.77 | 3.25 | 0.69 | 4.82 | 0.1 | 16.84 | 21.33 | 0.38 |
| 6 / 27 . | 52.41 | 0.81 | 3.57 | 0.78 | 4.55 | 0.11 | 16.55 | 21.69 | 0.38 |
| 6 / 28 . | 52.35 | 0.82 | 3.61 | 0.62 | 4.82 | 0.1 | 16.73 | 21.52 | 0.36 |
| 6 / 29 . | 52.74 | 0.73 | 3.02 | 0.63 | 4.57 | 0.09 | 16.82 | 21.93 | 0.37 |
| 6 / 30 . | 52.3 | 0.79 | 3.1 | 0.69 | 4.63 | 0.08 | 16.73 | 21.87 | 0.35 |

| Sample 1 | $SiO_2$ | $TiO_3$ | $Al_2O_4$ | $Cr_2O_4$ | FeO | MnO | MgO | CaO | $Na_2O$ |
|---|---|---|---|---|---|---|---|---|---|
| 3 / 1 . | 49.91 | 1.43 | 5.27 | 0.77 | 5.9 | 0.09 | 14.68 | 21.88 | 0.39 |
| 3 / 2 . | 52.49 | 0.67 | 3.44 | 0.72 | 4.81 | 0.14 | 17.21 | 20.72 | 0.37 |
| 3 / 3 . | 51.26 | 1 | 4.49 | 0.71 | 4.97 | 0.12 | 16.66 | 20.61 | 0.38 |
| 3 / 4 . | 49.44 | 1.17 | 5.12 | 0.78 | 5.94 | 0.14 | 15.57 | 20.62 | 0.42 |
| 3 / 5 . | 49.79 | 1.39 | 6.43 | 0.66 | 6.66 | 0.15 | 14.71 | 21.05 | 0.5 |
| 3 / 6 . | 49.57 | 1.35 | 6 | 0.74 | 6.34 | 0.14 | 14.72 | 20.87 | 0.5 |
| 3 / 7 . | 49.65 | 1.46 | 5.85 | 0.69 | 6.12 | 0.13 | 14.69 | 21.37 | 0.45 |
| 3 / 8 . | 48.74 | 1.79 | 7.14 | 0.6 | 6.83 | 0.15 | 13.85 | 21.23 | 0.52 |
| 3 / 10 . | 49.69 | 1.47 | 6.07 | 0.69 | 6.63 | 0.1 | 14.76 | 20.86 | 0.47 |
| 3 / 11 . | 49.71 | 1.39 | 6.05 | 0.71 | 6.76 | 0.13 | 14.88 | 20.75 | 0.48 |
| 3 / 12 . | 49.72 | 1.48 | 6.01 | 0.63 | 6.45 | 0.13 | 14.58 | 21.09 | 0.46 |
| 3 / 13 . | 49.5 | 1.61 | 6.56 | 0.66 | 6.68 | 0.11 | 14.47 | 20.99 | 0.49 |
| 3 / 14 . | 49.52 | 1.38 | 6.2 | 0.61 | 6.55 | 0.12 | 14.8 | 21.01 | 0.49 |
| 3 / 15 . | 49.65 | 1.48 | 6.12 | 0.66 | 6.47 | 0.12 | 14.67 | 21.14 | 0.47 |
| 3 / 16 . | 49.46 | 1.51 | 6.34 | 0.66 | 6.77 | 0.12 | 14.46 | 21.11 | 0.49 |
| 3 / 17 . | 49.53 | 1.6 | 6.22 | 0.71 | 6.72 | 0.12 | 14.66 | 21.19 | 0.47 |
| 3 / 18 . | 49.42 | 1.48 | 6.23 | 0.68 | 6.47 | 0.14 | 14.64 | 21.37 | 0.44 |
| 3 / 19 . | 49.26 | 1.49 | 6.52 | 0.64 | 6.65 | 0.1 | 14.44 | 21.15 | 0.5 |
| 3 / 20 . | 48.67 | 1.83 | 7.08 | 0.62 | 6.86 | 0.12 | 14.13 | 21.09 | 0.5 |
| 3 / 21 . | 49.98 | 1.48 | 6.16 | 0.67 | 6.62 | 0.12 | 14.68 | 21.03 | 0.49 |
| 3 / 22 . | 49.8 | 1.54 | 6.11 | 0.71 | 6.51 | 0.13 | 14.57 | 21.05 | 0.47 |
| 3 / 23 . | 50.08 | 1.44 | 6.04 | 0.69 | 6.44 | 0.15 | 14.72 | 21.02 | 0.46 |
| 3 / 24 . | 49.49 | 1.54 | 6.36 | 0.6 | 6.67 | 0.11 | 14.52 | 21.09 | 0.49 |
| 3 / 25 . | 49.86 | 1.51 | 6.11 | 0.63 | 6.59 | 0.13 | 14.54 | 21.23 | 0.49 |
| 3 / 26 . | 50.11 | 1.45 | 5.72 | 0.71 | 6.18 | 0.09 | 14.78 | 21.79 | 0.42 |
| 3 / 27 . | 50.52 | 1.27 | 5 | 0.74 | 5.88 | 0.11 | 15.08 | 21.95 | 0.39 |
| 3 / 28 . | 52.7 | 0.58 | 3.27 | 0.85 | 5.24 | 0.13 | 16.67 | 21.47 | 0.39 |
| 3 / 29 . | 51.11 | 0.63 | 3.43 | 0.89 | 4.5 | 0.09 | 16.98 | 20.82 | 0.36 |
| 3 / 30 . | 49.56 | 1.34 | 5.59 | 0.65 | 5.88 | 0.1 | 14.97 | 21.82 | 0.39 |

*Appendix III*

Small interval transects microprobe data as reported by analytical software.

| Sample 2 | $SiO_2$ | $TiO_2$ | $Al_2O3$ | $Cr_2O_3$ | FeO | MnO | MgO | CaO | $Na_2O$ |
|---|---|---|---|---|---|---|---|---|---|
| 1 / 1 . | 50.16 | 1.1 | 5.45 | 0.57 | 5.92 | 0.12 | 15.49 | 20.8 | 0.39 |
| 1 / 2 . | 50.79 | 0.95 | 4.88 | 0.56 | 5.93 | 0.1 | 15.64 | 20.66 | 0.38 |
| 1 / 3 . | 51.1 | 0.98 | 4.87 | 0.55 | 5.82 | 0.1 | 15.9 | 20.84 | 0.39 |
| 1 / 4 . | 50.97 | 0.96 | 4.71 | 0.62 | 5.85 | 0.08 | 16.03 | 20.71 | 0.39 |
| 1 / 5 . | 51.24 | 0.92 | 4.73 | 0.61 | 5.84 | 0.1 | 15.74 | 20.7 | 0.4 |
| 1 / 6 . | 50.51 | 1.03 | 4.87 | 0.69 | 5.78 | 0.11 | 15.88 | 20.49 | 0.38 |
| 1 / 7 . | 50.38 | 1.03 | 4.87 | 0.65 | 5.67 | 0.11 | 15.63 | 20.78 | 0.39 |
| 1 / 8 . | 50.5 | 0.93 | 4.75 | 0.6 | 5.97 | 0.11 | 16.05 | 20.66 | 0.4 |
| 1 / 9 . | 50.9 | 0.96 | 4.67 | 0.58 | 5.83 | 0.1 | 15.78 | 20.63 | 0.39 |
| 1 / 10 . | 50.39 | 0.97 | 4.73 | 0.61 | 5.87 | 0.1 | 15.87 | 20.7 | 0.4 |
| 1 / 11 . | 50.41 | 1 | 4.84 | 0.62 | 5.92 | 0.09 | 15.88 | 20.74 | 0.38 |
| 1 / 12 . | 50.2 | 1.08 | 5.24 | 0.5 | 5.95 | 0.12 | 15.42 | 20.73 | 0.41 |
| 1 / 13 . | 49.7 | 1.22 | 5.44 | 0.51 | 6.08 | 0.1 | 15.19 | 20.54 | 0.41 |
| 1 / 14 . | 49.92 | 1.23 | 5.45 | 0.47 | 6.14 | 0.12 | 15.15 | 20.56 | 0.43 |
| 1 / 15 . | 49.8 | 1.27 | 5.56 | 0.47 | 6.17 | 0.1 | 15.32 | 20.73 | 0.44 |
| 1 / 16 . | 48.94 | 1.45 | 6.51 | 0.53 | 6.37 | 0.13 | 14.9 | 20.58 | 0.48 |
| 1 / 17 . | 49.08 | 1.55 | 6.44 | 0.51 | 6.54 | 0.1 | 14.67 | 20.72 | 0.48 |
| 1 / 18 . | 48.6 | 1.54 | 6.59 | 0.48 | 6.49 | 0.11 | 14.77 | 20.51 | 0.5 |
| 1 / 19 . | 48.75 | 1.47 | 6.45 | 0.49 | 6.44 | 0.14 | 14.62 | 20.43 | 0.47 |
| 1 / 20 . | 48.75 | 1.56 | 6.72 | 0.49 | 6.5 | 0.12 | 14.57 | 20.5 | 0.47 |
| 1 / 21 . | 48.74 | 1.59 | 6.85 | 0.48 | 6.62 | 0.12 | 14.65 | 20.33 | 0.49 |
| 1 / 22 . | 48.46 | 1.47 | 6.73 | 0.51 | 6.53 | 0.11 | 14.78 | 20.15 | 0.49 |
| 1 / 23 . | 48.54 | 1.57 | 6.75 | 0.47 | 6.53 | 0.12 | 14.6 | 20.3 | 0.49 |
| 1 / 24 . | 48.58 | 1.57 | 6.77 | 0.47 | 6.59 | 0.13 | 14.51 | 20.32 | 0.48 |
| 1 / 25 . | 48.77 | 1.58 | 6.85 | 0.46 | 6.67 | 0.13 | 14.6 | 20.47 | 0.49 |
| 1 / 26 . | 49.03 | 1.55 | 6.83 | 0.44 | 6.86 | 0.11 | 14.61 | 20.19 | 0.48 |
| 1 / 27 . | 48.75 | 1.62 | 7.02 | 0.48 | 6.71 | 0.09 | 14.46 | 20.46 | 0.5 |
| 1 / 28 . | 49.17 | 1.55 | 6.96 | 0.5 | 6.61 | 0.13 | 14.78 | 20.2 | 0.5 |
| 1 / 34 . | 49.54 | 1.27 | 4.33 | 0.76 | 5.37 | 0.08 | 15.55 | 21.24 | 0.3 |
| 1 / 35 . | 48.05 | 1.54 | 6.69 | 0.57 | 6.69 | 0.1 | 14.36 | 20.48 | 0.5 |
| 1 / 36 . | 48.38 | 1.6 | 6.77 | 0.57 | 6.62 | 0.13 | 14.48 | 20.38 | 0.48 |
| 1 / 37 . | 48.49 | 1.48 | 6.5 | 0.55 | 6.52 | 0.12 | 14.62 | 20.55 | 0.5 |
| 1 / 38 . | 49.47 | 1.4 | 6.01 | 0.56 | 6.39 | 0.06 | 14.84 | 20.39 | 0.44 |
| 1 / 39 . | 50.24 | 1.2 | 5.58 | 0.51 | 5.9 | 0.1 | 15.28 | 20.77 | 0.4 |

| Sample 2 | $SiO_2$ | $TiO_2$ | $Al_2O3$ | $Cr_2O_3$ | FeO | MnO | MgO | CaO | $Na_2O$ |
|---|---|---|---|---|---|---|---|---|---|
| 1 / 40 . | 49.95 | 1.1 | 5.39 | 0.46 | 5.86 | 0.13 | 15.26 | 20.97 | 0.38 |
| 1 / 41 . | 49.97 | 1.1 | 5.43 | 0.56 | 5.93 | 0.15 | 15.39 | 20.82 | 0.37 |
| 1 / 42 . | 49.96 | 1.15 | 5.29 | 0.55 | 5.75 | 0.1 | 15.38 | 21.02 | 0.39 |
| 1 / 43 . | 49.94 | 1.15 | 5.23 | 0.6 | 5.91 | 0.12 | 15.36 | 20.84 | 0.38 |
| 1 / 44 . | 50.17 | 1.1 | 5.27 | 0.59 | 5.88 | 0.13 | 15.37 | 20.92 | 0.39 |
| 1 / 45 . | 49.9 | 1.07 | 5.28 | 0.64 | 5.82 | 0.1 | 15.61 | 21.07 | 0.38 |
| 1 / 46 . | 49.51 | 1.17 | 5.24 | 0.66 | 5.85 | 0.15 | 15.51 | 21.01 | 0.38 |
| 1 / 47 . | 49.83 | 1.04 | 5.25 | 0.66 | 5.93 | 0.07 | 15.38 | 20.75 | 0.4 |
| 1 / 48 . | 48.86 | 1.36 | 6.14 | 0.57 | 6.36 | 0.13 | 14.65 | 20.59 | 0.43 |
| 1 / 49 . | 48 | 1.65 | 7.28 | 0.45 | 6.78 | 0.15 | 13.98 | 20.6 | 0.52 |
| 1 / 50 . | 47.97 | 1.79 | 7.27 | 0.46 | 6.87 | 0.14 | 14.06 | 20.44 | 0.51 |
| 1 / 51 . | 48.37 | 1.77 | 7.33 | 0.46 | 6.8 | 0.13 | 13.92 | 20.6 | 0.49 |
| 1 / 52 . | 48.35 | 1.68 | 6.91 | 0.42 | 6.8 | 0.15 | 13.9 | 20.67 | 0.49 |
| 1 / 53 . | 48.77 | 1.58 | 6.98 | 0.55 | 6.61 | 0.12 | 14.14 | 20.54 | 0.5 |
| 1 / 54 . | 48.74 | 1.63 | 6.87 | 0.43 | 6.66 | 0.17 | 14.04 | 20.58 | 0.5 |
| 1 / 55 . | 48 | 1.65 | 7.06 | 0.43 | 6.79 | 0.13 | 13.97 | 20.76 | 0.51 |
| 1 / 56 . | 48.56 | 1.73 | 6.88 | 0.52 | 6.73 | 0.11 | 13.81 | 20.94 | 0.49 |
| 1 / 57 . | 47.86 | 1.83 | 7.15 | 0.5 | 6.72 | 0.12 | 14.05 | 20.71 | 0.5 |
| 1 / 58 . | 48.22 | 1.7 | 6.99 | 0.48 | 6.69 | 0.13 | 13.9 | 20.87 | 0.51 |
| 1 / 59 . | 48.35 | 1.75 | 7 | 0.44 | 6.75 | 0.12 | 14.05 | 20.87 | 0.51 |
| 1 / 60 . | 48.63 | 1.64 | 6.96 | 0.45 | 6.79 | 0.1 | 14.05 | 21.03 | 0.5 |
| 1 / 61 . | 48.64 | 1.58 | 6.75 | 0.5 | 6.54 | 0.12 | 14.2 | 20.99 | 0.48 |
| 1 / 62 . | 49.16 | 1.4 | 5.9 | 0.43 | 6.14 | 0.1 | 14.62 | 21.1 | 0.43 |
| 1 / 63 . | 49.59 | 1.36 | 6.06 | 0.54 | 6.16 | 0.13 | 14.81 | 21.1 | 0.44 |
| 1 / 64 . | 49.58 | 1.42 | 6 | 0.52 | 6.14 | 0.12 | 14.64 | 21.4 | 0.44 |
| 1 / 65 . | 49.63 | 1.36 | 6.08 | 0.49 | 6.17 | 0.15 | 14.6 | 21.56 | 0.44 |
| 1 / 66 . | 49.18 | 1.41 | 6.09 | 0.47 | 6.15 | 0.13 | 14.69 | 21.22 | 0.43 |
| 1 / 67 . | 49.45 | 1.5 | 6.3 | 0.46 | 6.22 | 0.08 | 14.76 | 21.39 | 0.43 |
| 1 / 68 . | 49.49 | 1.47 | 6.26 | 0.48 | 6.2 | 0.08 | 14.79 | 21.32 | 0.44 |
| 1 / 69 . | 49.06 | 1.49 | 6.2 | 0.45 | 6.23 | 0.13 | 14.52 | 21.29 | 0.43 |
| 1 / 70 . | 48.96 | 1.46 | 6.16 | 0.52 | 6.3 | 0.12 | 14.56 | 21.22 | 0.45 |
| 1 / 71 . | 48.73 | 1.48 | 6.19 | 0.51 | 6.25 | 0.13 | 14.38 | 21.37 | 0.44 |
| 1 / 72 . | 49.4 | 1.46 | 6.27 | 0.47 | 6.3 | 0.1 | 14.52 | 21.32 | 0.45 |
| 1 / 73 . | 49.5 | 1.53 | 6.45 | 0.53 | 6.37 | 0.08 | 14.56 | 21.38 | 0.47 |
| 1 / 74 . | 49.05 | 1.53 | 6.46 | 0.46 | 6.52 | 0.11 | 14.27 | 21.24 | 0.46 |
| 1 / 75 . | 48.87 | 1.53 | 6.42 | 0.54 | 6.28 | 0.11 | 14.7 | 21.31 | 0.47 |
| 1 / 76 . | 49.43 | 1.52 | 6.34 | 0.53 | 6.23 | 0.09 | 14.28 | 21.21 | 0.47 |
| 1 / 77 . | 48.83 | 1.49 | 6.39 | 0.49 | 6.27 | 0.1 | 14.44 | 21.05 | 0.45 |

| Sample 2 | $SiO_2$ | $TiO_2$ | $Al_2O3$ | $Cr_2O_3$ | FeO | MnO | MgO | CaO | $Na_2O$ |
|---|---|---|---|---|---|---|---|---|---|
| 1 / 78 . | 48.67 | 1.52 | 6.27 | 0.5 | 6.25 | 0.11 | 14.35 | 21.3 | 0.46 |
| 1 / 79 . | 49.09 | 1.44 | 6.39 | 0.53 | 6.25 | 0.12 | 14.61 | 21.16 | 0.48 |
| 1 / 80 . | 49.05 | 1.54 | 6.27 | 0.53 | 6.3 | 0.1 | 14.37 | 21.27 | 0.47 |
| 1 / 81 . | 49.17 | 1.46 | 6.4 | 0.54 | 6.28 | 0.11 | 14.49 | 21.04 | 0.47 |
| 1 / 82 . | 48.77 | 1.54 | 6.29 | 0.53 | 6.11 | 0.11 | 14.59 | 21.42 | 0.44 |
| 1 / 83 . | 49.56 | 1.32 | 5.96 | 0.57 | 5.93 | 0.12 | 14.88 | 21.35 | 0.41 |
| 1 / 84 . | 50.63 | 1.09 | 5.1 | 0.65 | 5.84 | 0.12 | 15.21 | 21.35 | 0.4 |
| 1 / 85 . | 50.44 | 1.09 | 5.13 | 0.64 | 5.71 | 0.11 | 15.42 | 21.5 | 0.38 |
| 1 / 86 . | 50.47 | 1.08 | 4.94 | 0.57 | 5.78 | 0.08 | 15.38 | 21.39 | 0.38 |
| 1 / 87 . | 50.03 | 1.08 | 5.01 | 0.61 | 5.62 | 0.11 | 15.34 | 21.32 | 0.39 |
| 1 / 88 . | 50.35 | 1.06 | 5.05 | 0.66 | 5.73 | 0.12 | 15.19 | 21.41 | 0.38 |
| 1 / 89 . | 50.65 | 1.09 | 5.21 | 0.57 | 5.72 | 0.11 | 15.11 | 21.58 | 0.37 |
| 1 / 90 . | 50.03 | 1.09 | 5.15 | 0.6 | 5.87 | 0.09 | 15.14 | 21.43 | 0.38 |
| 1 / 91 . | 48.29 | 1.65 | 7.06 | 0.49 | 6.59 | 0.1 | 14.03 | 21.22 | 0.46 |
| 1 / 92 . | 48.14 | 1.72 | 7.23 | 0.48 | 6.77 | 0.09 | 13.92 | 20.96 | 0.5 |
| 1 / 93 . | 48.19 | 1.79 | 7.11 | 0.47 | 6.84 | 0.12 | 13.94 | 21.02 | 0.5 |
| 1 / 94 . | 48.49 | 1.63 | 7.08 | 0.47 | 6.73 | 0.12 | 14.26 | 20.96 | 0.5 |
| 1 / 95 . | 50.23 | 1.08 | 5.29 | 0.66 | 5.97 | 0.11 | 15.14 | 21.34 | 0.4 |
| 1 / 96 . | 50.35 | 1.17 | 4.93 | 0.75 | 5.62 | 0.09 | 15.2 | 21.5 | 0.36 |
| 1 / 97 . | 50.53 | 1.13 | 4.98 | 0.63 | 5.74 | 0.09 | 15.56 | 21.62 | 0.38 |
| 1 / 98 . | 50.38 | 1.09 | 5.16 | 0.65 | 5.68 | 0.11 | 15.27 | 21.62 | 0.36 |
| 1 / 99 . | 50.93 | 1.09 | 5.01 | 0.64 | 5.72 | 0.1 | 15.37 | 21.46 | 0.38 |
| 1 / 100 . | 50.47 | 1.06 | 4.9 | 0.7 | 5.82 | 0.09 | 15.29 | 21.61 | 0.37 |
| 1 / 101 . | 50.18 | 1.13 | 5.09 | 0.64 | 5.92 | 0.09 | 15.79 | 21.64 | 0.38 |
| 1 / 102 . | 50.33 | 1.09 | 5.07 | 0.62 | 5.78 | 0.13 | 15.57 | 21.73 | 0.39 |
| 1 / 103 . | 50.25 | 1.1 | 5.21 | 0.65 | 5.8 | 0.12 | 15.56 | 21.59 | 0.38 |
| 1 / 104 . | 50.02 | 1.12 | 5.25 | 0.64 | 5.71 | 0.11 | 15.54 | 21.68 | 0.38 |
| 1 / 105 . | 50.12 | 1.13 | 5.32 | 0.59 | 5.8 | 0.1 | 15.53 | 21.6 | 0.39 |
| 1 / 106 . | 50.4 | 1.12 | 5.18 | 0.64 | 5.85 | 0.08 | 15.32 | 21.52 | 0.39 |
| 1 / 107 . | 50.37 | 1.07 | 5.26 | 0.64 | 5.84 | 0.09 | 15.49 | 21.38 | 0.4 |
| 1 / 108 . | 50.33 | 1.08 | 5.18 | 0.67 | 5.82 | 0.11 | 15.29 | 21.58 | 0.37 |
| 1 / 109 . | 50.28 | 1.09 | 5.21 | 0.67 | 5.72 | 0.11 | 15.43 | 21.53 | 0.37 |
| 1 / 110 . | 50.39 | 1.17 | 5.25 | 0.6 | 5.85 | 0.11 | 15.52 | 21.75 | 0.38 |
| 1 / 112 . | 50.44 | 1.1 | 5.17 | 0.67 | 5.76 | 0.09 | 15.5 | 21.59 | 0.39 |
| 1 / 113 . | 50.13 | 1.13 | 5.4 | 0.73 | 5.95 | 0.1 | 15.48 | 21.35 | 0.38 |
| 1 / 114 . | 50.28 | 1.08 | 5.27 | 0.64 | 5.95 | 0.1 | 15.39 | 21.43 | 0.4 |
| 1 / 115 . | 47.99 | 1.74 | 7.06 | 0.52 | 6.8 | 0.12 | 14.29 | 21.35 | 0.49 |
| 1 / 116 . | 48.64 | 1.75 | 7.3 | 0.51 | 6.89 | 0.14 | 14.1 | 20.98 | 0.54 |

| Sample 2 | $SiO_2$ | $TiO_2$ | $Al_2O3$ | $Cr_2O_3$ | FeO | MnO | MgO | CaO | $Na_2O$ |
|---|---|---|---|---|---|---|---|---|---|
| 1 / 117 . | 48.72 | 1.73 | 7.21 | 0.44 | 6.95 | 0.11 | 14.24 | 21.38 | 0.51 |
| 1 / 118 . | 49.49 | 1.54 | 6.43 | 0.59 | 6.6 | 0.09 | 14.71 | 21.29 | 0.49 |
| 1 / 119 . | 50.34 | 1.05 | 5.04 | 0.62 | 5.9 | 0.1 | 15.6 | 21.26 | 0.41 |
| 1 / 120 . | 50.95 | 1.13 | 5.04 | 0.51 | 5.95 | 0.08 | 15.78 | 21.58 | 0.39 |
| 1 / 121 . | 50.69 | 1.06 | 5.04 | 0.4 | 5.86 | 0.1 | 15.61 | 21.46 | 0.4 |
| 1 / 122 . | 50.31 | 1.29 | 5.5 | 0.54 | 6.24 | 0.09 | 15.26 | 21.64 | 0.43 |
| 1 / 123 . | 48.37 | 1.69 | 7.15 | 0.48 | 6.8 | 0.14 | 14.25 | 21.14 | 0.5 |
| 1 / 124 . | 48.43 | 1.74 | 7.02 | 0.46 | 6.73 | 0.09 | 14.37 | 21.05 | 0.5 |
| 1 / 125 . | 48.46 | 1.6 | 6.9 | 0.48 | 6.7 | 0.12 | 14.48 | 21.35 | 0.48 |
| 1 / 126 . | 48.91 | 1.75 | 6.98 | 0.5 | 6.72 | 0.11 | 14.44 | 21.2 | 0.5 |
| 1 / 127 . | 48.75 | 1.7 | 7.26 | 0.51 | 6.78 | 0.13 | 14.38 | 21.29 | 0.51 |
| 1 / 128 . | 48.16 | 1.77 | 7.21 | 0.44 | 6.88 | 0.08 | 14.13 | 20.98 | 0.52 |
| 1 / 129 . | 48.17 | 1.81 | 7.39 | 0.47 | 6.84 | 0.12 | 14.28 | 21.04 | 0.5 |
| 1 / 130 . | 48.43 | 1.73 | 7.21 | 0.49 | 6.76 | 0.12 | 14.24 | 21.12 | 0.5 |
| 1 / 131 . | 48.44 | 1.72 | 7.29 | 0.54 | 6.97 | 0.1 | 14.2 | 21.12 | 0.5 |
| 1 / 132 . | 48.49 | 1.8 | 7.27 | 0.47 | 6.86 | 0.11 | 14.17 | 21.17 | 0.49 |
| 1 / 133 . | 48.26 | 1.76 | 7.19 | 0.51 | 6.91 | 0.12 | 14.43 | 21.01 | 0.5 |
| 1 / 134 . | 48.38 | 1.74 | 7.26 | 0.45 | 6.91 | 0.1 | 14.2 | 21.06 | 0.5 |
| 1 / 135 . | 48.31 | 1.78 | 7.19 | 0.47 | 6.8 | 0.14 | 14.26 | 21.24 | 0.49 |
| 1 / 136 . | 48.35 | 1.8 | 7.15 | 0.45 | 6.77 | 0.09 | 14.21 | 21.07 | 0.49 |
| 1 / 137 . | 48.73 | 1.73 | 6.87 | 0.5 | 6.68 | 0.08 | 14.34 | 21.13 | 0.49 |
| 1 / 138 . | 49.46 | 1.37 | 5.84 | 0.55 | 6.35 | 0.13 | 14.9 | 21.21 | 0.46 |
| 1 / 139 . | 50.05 | 1.16 | 5.59 | 0.67 | 5.81 | 0.13 | 15.28 | 21.59 | 0.39 |
| 1 / 140 . | 50.38 | 1.09 | 5.29 | 0.67 | 5.8 | 0.14 | 15.51 | 21.48 | 0.38 |
| 1 / 141 . | 50.29 | 1.09 | 5.29 | 0.65 | 5.76 | 0.12 | 15.41 | 21.36 | 0.38 |
| 1 / 143 . | 50.04 | 1.1 | 5.24 | 0.66 | 5.91 | 0.08 | 15.76 | 21.62 | 0.39 |
| 1 / 144 . | 50.26 | 1.1 | 5.3 | 0.64 | 5.78 | 0.08 | 15.74 | 21.59 | 0.37 |
| 1 / 145 . | 50.37 | 1.06 | 5.26 | 0.65 | 5.82 | 0.11 | 15.44 | 21.58 | 0.37 |
| 1 / 146 . | 50.31 | 1.1 | 5.3 | 0.58 | 5.92 | 0.11 | 15.54 | 21.29 | 0.4 |
| 1 / 147 . | 50.32 | 1.06 | 5.32 | 0.57 | 5.78 | 0.1 | 15.67 | 21.55 | 0.4 |
| 1 / 148 . | 50.65 | 1.09 | 5.21 | 0.7 | 5.69 | 0.12 | 15.57 | 21.65 | 0.38 |
| 1 / 149 . | 50.71 | 1.15 | 5.21 | 0.64 | 5.71 | 0.13 | 15.41 | 21.55 | 0.4 |
| 1 / 150 . | 50.48 | 1.06 | 5.07 | 0.65 | 5.83 | 0.14 | 15.54 | 21.65 | 0.4 |

| Sample 6 | $SiO_2$ | $TiO_2$ | $Al_2O3$ | $Cr_2O_3$ | FeO | MnO | MgO | CaO | $Na_2O$ |
|---|---|---|---|---|---|---|---|---|---|
| 1 / 1 . | 50.6 | 1.06 | 4.92 | 0.81 | 5.9 | 0.14 | 15.85 | 20.67 | 0.4 |
| 1 / 2 . | 50.53 | 1.18 | 4.89 | 0.8 | 5.95 | 0.1 | 15.83 | 20.86 | 0.4 |
| 1 / 3 . | 50.21 | 1.1 | 4.85 | 0.76 | 5.87 | 0.14 | 15.66 | 20.91 | 0.42 |
| 1 / 4 . | 51.1 | 1.11 | 4.92 | 0.79 | 5.89 | 0.09 | 15.84 | 20.76 | 0.39 |
| 1 / 5 . | 50.75 | 1.18 | 5 | 0.78 | 5.81 | 0.12 | 15.89 | 20.84 | 0.39 |
| 1 / 6 . | 50.82 | 1.16 | 5.09 | 0.78 | 5.76 | 0.12 | 15.87 | 20.88 | 0.4 |
| 1 / 7 . | 50.63 | 1.18 | 5.11 | 0.8 | 5.84 | 0.09 | 15.92 | 20.86 | 0.4 |
| 1 / 8 . | 50.65 | 1.1 | 5.06 | 0.86 | 5.78 | 0.08 | 16.01 | 20.98 | 0.4 |
| 1 / 9 . | 50.68 | 1.08 | 5.04 | 0.81 | 5.61 | 0.12 | 15.93 | 20.85 | 0.41 |
| 1 / 10 . | 50.85 | 1.09 | 4.98 | 0.83 | 5.45 | 0.09 | 15.92 | 20.96 | 0.41 |
| 1 / 11 . | 51.48 | 1.03 | 4.56 | 0.81 | 5.42 | 0.11 | 16.17 | 20.8 | 0.41 |
| 1 / 12 . | 50.76 | 1.04 | 4.8 | 0.9 | 5.38 | 0.11 | 16.09 | 20.76 | 0.41 |
| 1 / 13 . | 50.63 | 1.03 | 4.92 | 0.96 | 5.35 | 0.1 | 16.2 | 20.73 | 0.42 |
| 1 / 14 . | 50.68 | 1.1 | 5.03 | 0.96 | 5.35 | 0.14 | 16.15 | 20.89 | 0.4 |
| 1 / 15 . | 50.62 | 1.07 | 4.62 | 0.92 | 5.21 | 0.15 | 16.11 | 20.67 | 0.41 |
| 1 / 16 . | 51.52 | 0.84 | 4.2 | 1.01 | 5.06 | 0.1 | 16.4 | 20.91 | 0.4 |
| 1 / 17 . | 51.46 | 0.85 | 4.12 | 1.08 | 4.88 | 0.16 | 16.51 | 21.03 | 0.39 |
| 1 / 18 . | 51.47 | 0.81 | 4.07 | 1.11 | 4.83 | 0.09 | 16.43 | 21.31 | 0.4 |
| 1 / 19 . | 51.5 | 0.84 | 4.07 | 1.06 | 4.84 | 0.09 | 16.42 | 21.03 | 0.4 |
| 1 / 20 . | 51.77 | 0.82 | 4.11 | 1.05 | 4.77 | 0.11 | 16.41 | 21.07 | 0.38 |
| 1 / 21 . | 51.98 | 0.85 | 3.94 | 1.15 | 4.78 | 0.1 | 16.48 | 21.23 | 0.4 |
| 1 / 22 . | 52.16 | 0.83 | 4.11 | 1.01 | 4.82 | 0.11 | 16.4 | 21.04 | 0.38 |
| 1 / 23 . | 52.12 | 0.81 | 4.1 | 1.11 | 4.75 | 0.09 | 16.64 | 21.01 | 0.37 |
| 1 / 24 . | 52.2 | 0.77 | 4.12 | 1.07 | 4.78 | 0.05 | 16.63 | 21.22 | 0.4 |
| 1 / 25 . | 51.96 | 0.83 | 4.03 | 1.08 | 4.75 | 0.1 | 16.57 | 21.09 | 0.39 |
| 1 / 26 . | 50.88 | 0.81 | 4 | 1.05 | 4.74 | 0.09 | 15.9 | 21.14 | 0.4 |
| 1 / 27 . | 51.75 | 0.88 | 4.11 | 1.07 | 4.75 | 0.12 | 16.47 | 21.47 | 0.39 |
| 1 / 28 . | 52.1 | 0.92 | 4.14 | 1.09 | 4.82 | 0.08 | 16.62 | 21.29 | 0.39 |
| 1 / 29 . | 52.02 | 0.8 | 4.15 | 1.11 | 4.73 | 0.1 | 16.57 | 21.12 | 0.38 |
| 1 / 30 . | 51.51 | 0.85 | 4.07 | 1.08 | 4.84 | 0.07 | 16.53 | 21.23 | 0.4 |
| 1 / 31 . | 51.51 | 0.8 | 4.1 | 1.14 | 4.76 | 0.11 | 16.33 | 21.32 | 0.39 |
| 1 / 32 . | 51.44 | 0.9 | 4.03 | 1.05 | 4.81 | 0.12 | 16.38 | 21.28 | 0.39 |
| 1 / 33 . | 51.39 | 0.89 | 4.06 | 1.03 | 4.77 | 0.06 | 16.39 | 21.2 | 0.38 |
| 1 / 34 . | 51.44 | 0.84 | 3.98 | 1.06 | 4.7 | 0.11 | 16.45 | 21.33 | 0.39 |
| 1 / 35 . | 52.05 | 0.69 | 3.8 | 1.04 | 4.7 | 0.09 | 16.66 | 21.13 | 0.38 |
| 1 / 36 . | 52 | 0.8 | 3.67 | 0.98 | 4.67 | 0.07 | 16.7 | 21.31 | 0.38 |
| 1 / 37 . | 51.59 | 0.81 | 4.09 | 1.08 | 4.89 | 0.1 | 16.43 | 21.28 | 0.4 |

| Sample 6 | $SiO_2$ | $TiO_2$ | $Al_2O3$ | $Cr_2O_3$ | FeO | MnO | MgO | CaO | $Na_2O$ |
|---|---|---|---|---|---|---|---|---|---|
| 1 / 38 . | 51.35 | 0.87 | 4.18 | 1.1 | 4.77 | 0.1 | 16.41 | 20.97 | 0.4 |
| 1 / 39 . | 51.28 | 0.91 | 4.15 | 1.11 | 4.85 | 0.11 | 16.28 | 21.05 | 0.41 |
| 1 / 40 . | 50.99 | 0.85 | 4.14 | 1.1 | 4.95 | 0.11 | 16.21 | 21.14 | 0.4 |
| 1 / 41 . | 51.72 | 0.86 | 4.11 | 1.09 | 5.14 | 0.08 | 16.37 | 20.85 | 0.41 |
| 1 / 42 . | 51.37 | 0.97 | 4.16 | 0.96 | 5.2 | 0.11 | 16.34 | 20.73 | 0.42 |
| 1 / 43 . | 51.37 | 1.03 | 4.32 | 0.86 | 5.34 | 0.1 | 16.38 | 20.92 | 0.4 |
| 1 / 44 . | 50.95 | 1 | 4.73 | 0.87 | 5.49 | 0.07 | 16.01 | 20.28 | 0.5 |
| 1 / 46 . | 50.66 | 0.94 | 4.18 | 0.89 | 5.32 | 0.1 | 16.08 | 20.83 | 0.43 |
| 1 / 47 . | 50.62 | 1.03 | 4.71 | 0.85 | 5.47 | 0.11 | 16.15 | 20.83 | 0.4 |
| 1 / 48 . | 50.51 | 0.98 | 4.61 | 0.94 | 5.39 | 0.09 | 15.7 | 20.7 | 0.39 |
| 1 / 49 . | 51.09 | 0.92 | 4.61 | 0.89 | 5.47 | 0.06 | 16.15 | 20.9 | 0.39 |
| 1 / 50 . | 50.77 | 1.05 | 4.8 | 0.87 | 5.58 | 0.09 | 15.83 | 20.73 | 0.41 |
| 1 / 51 . | 50.71 | 1.13 | 4.85 | 0.87 | 5.49 | 0.11 | 15.84 | 20.71 | 0.39 |
| 1 / 52 . | 50.74 | 1.08 | 4.82 | 0.73 | 5.54 | 0.07 | 15.84 | 20.83 | 0.39 |
| 1 / 53 . | 50.49 | 1.06 | 4.9 | 0.91 | 5.5 | 0.14 | 16.13 | 20.45 | 0.4 |
| 1 / 54 . | 50.6 | 0.98 | 4.82 | 0.89 | 5.54 | 0.11 | 15.85 | 20.68 | 0.4 |
| 1 / 55 . | 50.55 | 0.92 | 4.75 | 0.89 | 5.54 | 0.07 | 16 | 20.48 | 0.41 |
| 1 / 56 . | 50.95 | 0.99 | 4.81 | 0.8 | 5.49 | 0.1 | 16.27 | 20.66 | 0.39 |
| 1 / 57 . | 51.21 | 0.93 | 4.88 | 0.88 | 5.62 | 0.09 | 16.31 | 20.53 | 0.38 |
| 1 / 58 . | 50.77 | 1.01 | 4.87 | 0.89 | 5.62 | 0.13 | 16.05 | 20.74 | 0.38 |
| 1 / 59 . | 50.71 | 1.05 | 4.91 | 0.8 | 5.61 | 0.1 | 15.92 | 20.75 | 0.37 |
| 1 / 60 . | 50.56 | 1.08 | 4.87 | 0.79 | 5.56 | 0.11 | 15.86 | 20.66 | 0.38 |
| 1 / 61 . | 50.67 | 1.1 | 4.97 | 0.85 | 5.66 | 0.11 | 15.77 | 20.78 | 0.39 |
| 1 / 62 . | 50.33 | 1.1 | 4.89 | 0.83 | 5.61 | 0.09 | 15.84 | 20.81 | 0.37 |
| 1 / 63 . | 50.92 | 0.98 | 4.68 | 0.79 | 5.56 | 0.12 | 15.98 | 20.43 | 0.39 |
| 1 / 64 . | 50.91 | 0.91 | 4.69 | 0.82 | 5.58 | 0.12 | 16.09 | 20.66 | 0.38 |
| 1 / 65 . | 50.75 | 1.01 | 4.66 | 0.87 | 5.61 | 0.09 | 16.06 | 20.42 | 0.39 |
| 1 / 66 . | 50.63 | 0.99 | 4.69 | 0.81 | 5.58 | 0.12 | 16.01 | 20.61 | 0.39 |
| 1 / 67 . | 50.81 | 0.99 | 4.77 | 0.87 | 5.7 | 0.09 | 15.94 | 20.86 | 0.4 |
| 1 / 68 . | 50.48 | 1.07 | 4.83 | 0.88 | 5.63 | 0.13 | 15.94 | 20.78 | 0.4 |
| 1 / 69 . | 50.49 | 1.1 | 4.91 | 0.78 | 5.62 | 0.12 | 15.83 | 20.76 | 0.39 |
| 1 / 70 . | 50.14 | 1.14 | 5.08 | 0.8 | 5.66 | 0.14 | 15.63 | 20.94 | 0.39 |
| 1 / 71 . | 50.23 | 1.02 | 4.97 | 0.79 | 5.56 | 0.14 | 15.93 | 20.57 | 0.41 |
| 1 / 72 . | 50.12 | 1.12 | 5.07 | 0.8 | 5.65 | 0.12 | 15.55 | 20.85 | 0.38 |
| 1 / 73 . | 49.84 | 1.05 | 5.13 | 0.77 | 5.77 | 0.09 | 15.76 | 20.8 | 0.38 |
| 1 / 74 . | 50.21 | 0.99 | 4.89 | 0.75 | 5.62 | 0.13 | 15.92 | 20.81 | 0.38 |
| 1 / 75 . | 50.61 | 1.18 | 4.86 | 0.87 | 5.67 | 0.11 | 15.7 | 20.68 | 0.39 |
| 1 / 76 . | 50.69 | 1.1 | 4.91 | 0.77 | 5.73 | 0.05 | 15.82 | 20.96 | 0.4 |

| Sample 6 | $SiO_2$ | $TiO_2$ | $Al_2O3$ | $Cr_2O_3$ | FeO | MnO | MgO | CaO | $Na_2O$ |
|---|---|---|---|---|---|---|---|---|---|
| 1 / 78 . | 50.56 | 1.09 | 5.11 | 0.79 | 5.78 | 0.12 | 15.56 | 20.53 | 0.44 |
| 1 / 79 . | 50.57 | 1.23 | 4.83 | 0.85 | 5.73 | 0.06 | 15.96 | 20.9 | 0.37 |
| 1 / 80 . | 50.54 | 1.1 | 4.78 | 0.75 | 5.79 | 0.1 | 16.04 | 21.07 | 0.38 |
| 1 / 81 . | 50.5 | 1.13 | 4.93 | 0.72 | 5.72 | 0.11 | 15.71 | 21.02 | 0.39 |
| 1 / 82 . | 50.79 | 1.17 | 4.91 | 0.74 | 5.66 | 0.11 | 16.02 | 20.78 | 0.38 |
| 1 / 83 . | 50.93 | 1.09 | 4.88 | 0.83 | 5.63 | 0.14 | 16.08 | 20.58 | 0.4 |
| 1 / 84 . | 50.96 | 1.08 | 4.76 | 0.87 | 5.66 | 0.12 | 15.9 | 20.88 | 0.38 |
| 1 / 85 . | 50.99 | 1.12 | 4.59 | 0.9 | 5.59 | 0.12 | 16.08 | 20.87 | 0.38 |
| 1 / 86 . | 51.17 | 0.95 | 4.42 | 0.93 | 5.42 | 0.1 | 16.36 | 20.93 | 0.39 |
| 1 / 88 . | 51.11 | 0.81 | 4.15 | 1 | 5.25 | 0.14 | 16.3 | 21.2 | 0.37 |
| 1 / 89 . | 51.78 | 0.85 | 4.26 | 1.08 | 5.09 | 0.11 | 16.4 | 21.29 | 0.38 |
| 1 / 90 . | 51.45 | 0.84 | 4.14 | 1.02 | 4.9 | 0.1 | 16.26 | 21.56 | 0.39 |
| 1 / 91 . | 51.49 | 0.8 | 4.14 | 1.09 | 4.68 | 0.1 | 16.37 | 21.24 | 0.4 |
| 1 / 92 . | 51.08 | 0.87 | 4.15 | 1.01 | 4.84 | 0.11 | 16.5 | 21.09 | 0.37 |
| 1 / 93 . | 51.25 | 0.92 | 4.16 | 1.02 | 4.66 | 0.09 | 16.31 | 21.36 | 0.39 |
| 1 / 94 . | 50.75 | 0.88 | 4.17 | 1.04 | 4.66 | 0.11 | 16.42 | 21.16 | 0.38 |
| 1 / 95 . | 51.42 | 0.88 | 4.12 | 1.05 | 4.77 | 0.09 | 16.41 | 21.19 | 0.38 |
| 1 / 96 . | 51.22 | 0.87 | 4.19 | 1.12 | 4.72 | 0.09 | 16.33 | 21.17 | 0.4 |
| 1 / 97 . | 51.27 | 0.87 | 4.37 | 1.12 | 4.8 | 0.09 | 16.3 | 21.02 | 0.41 |
| 1 / 98 . | 51.62 | 0.85 | 4.19 | 1.09 | 4.73 | 0.1 | 16.18 | 21.11 | 0.41 |
| 1 / 99 . | 51.31 | 0.84 | 4.3 | 1.06 | 4.67 | 0.1 | 16.39 | 21.02 | 0.39 |
| 1 / 100 . | 51.42 | 0.9 | 4.28 | 1.11 | 4.77 | 0.11 | 16.34 | 21.18 | 0.39 |
| 1 / 101 . | 51.41 | 0.85 | 4.23 | 1.11 | 4.72 | 0.07 | 16.41 | 21.09 | 0.39 |
| 1 / 102 . | 51.35 | 0.83 | 4.16 | 1.13 | 4.76 | 0.09 | 16.5 | 21.06 | 0.39 |
| 1 / 103 . | 51.47 | 0.89 | 4.23 | 1.1 | 4.6 | 0.07 | 16.4 | 20.89 | 0.39 |
| 1 / 104 . | 51.72 | 0.75 | 4.24 | 1.05 | 4.7 | 0.1 | 16.23 | 20.99 | 0.4 |
| 1 / 105 . | 51.26 | 0.92 | 4.17 | 1.15 | 4.76 | 0.07 | 16.37 | 21.08 | 0.38 |
| 1 / 106 . | 51.62 | 0.87 | 4.27 | 1.08 | 4.77 | 0.04 | 16.31 | 21.15 | 0.39 |
| 1 / 107 . | 51.59 | 0.83 | 4.15 | 1.08 | 4.79 | 0.09 | 16.46 | 21.09 | 0.4 |
| 1 / 108 . | 51.41 | 0.83 | 4.11 | 1.04 | 4.72 | 0.06 | 16.4 | 20.99 | 0.39 |
| 1 / 109 . | 51.94 | 0.79 | 3.83 | 0.91 | 4.67 | 0.13 | 16.74 | 21.07 | 0.39 |
| 1 / 110 . | 52.3 | 0.77 | 3.88 | 0.9 | 4.76 | 0.08 | 16.78 | 21.4 | 0.36 |
| 1 / 111 . | 51.91 | 0.84 | 4.02 | 0.93 | 4.74 | 0.11 | 16.39 | 21.26 | 0.39 |
| 1 / 112 . | 51.55 | 0.85 | 4.12 | 1.01 | 4.74 | 0.06 | 16.47 | 21.02 | 0.38 |
| 1 / 113 . | 51.23 | 0.87 | 4.12 | 1.08 | 4.66 | 0.13 | 16.18 | 21.35 | 0.38 |
| 1 / 114 . | 51.29 | 0.91 | 4.17 | 1.07 | 4.68 | 0.06 | 16.31 | 21.15 | 0.38 |
| 1 / 115 . | 51.31 | 0.86 | 4.2 | 1.08 | 4.65 | 0.1 | 16.48 | 21.31 | 0.39 |
| 1 / 116 . | 51.69 | 0.81 | 3.92 | 0.97 | 4.74 | 0.1 | 16.44 | 21.33 | 0.37 |

| Sample 6 | $SiO_2$ | $TiO_2$ | $Al_2O3$ | $Cr_2O_3$ | FeO | MnO | MgO | CaO | $Na_2O$ |
|---|---|---|---|---|---|---|---|---|---|
| 1 / 117 . | 51.59 | 0.86 | 3.89 | 0.98 | 4.74 | 0.07 | 16.4 | 21.23 | 0.38 |
| 1 / 118 . | 51.51 | 0.91 | 3.85 | 1.01 | 4.79 | 0.13 | 16.37 | 21.22 | 0.36 |
| 1 / 119 . | 51.66 | 0.85 | 3.85 | 0.98 | 4.74 | 0.09 | 16.51 | 21.4 | 0.37 |
| 1 / 120 . | 51.83 | 0.79 | 3.68 | 0.95 | 4.86 | 0.1 | 16.75 | 21.19 | 0.37 |
| 1 / 121 . | 51.78 | 0.75 | 3.66 | 1.08 | 4.72 | 0.1 | 16.67 | 21.16 | 0.37 |
| 1 / 122 . | 51.7 | 0.8 | 3.61 | 1 | 4.78 | 0.11 | 16.5 | 21.24 | 0.38 |
| 1 / 123 . | 51.49 | 0.81 | 3.86 | 0.92 | 4.64 | 0.08 | 16.57 | 21.24 | 0.36 |
| 1 / 124 . | 51.57 | 0.86 | 4.03 | 1.05 | 4.83 | 0.12 | 16.56 | 21.35 | 0.39 |
| 1 / 125 . | 51.53 | 0.84 | 4.08 | 1.09 | 4.85 | 0.08 | 16.32 | 21.26 | 0.38 |
| 1 / 126 . | 51.24 | 0.86 | 4.08 | 1.1 | 4.9 | 0.1 | 16.26 | 21.17 | 0.38 |
| 1 / 127 . | 51.23 | 0.9 | 4.29 | 1.08 | 4.92 | 0.13 | 16.35 | 21.1 | 0.39 |
| 1 / 128 . | 51.32 | 0.87 | 4.19 | 1.07 | 4.93 | 0.12 | 16.38 | 21.15 | 0.38 |
| 1 / 129 . | 51.15 | 0.92 | 4.13 | 1.05 | 4.97 | 0.09 | 16.3 | 21.01 | 0.38 |
| 1 / 130 . | 51.43 | 0.84 | 4.18 | 1.04 | 4.96 | 0.13 | 16.23 | 21.28 | 0.38 |
| 1 / 132 . | 51.28 | 0.86 | 4.08 | 0.97 | 4.85 | 0.13 | 16.32 | 21.24 | 0.38 |
| 1 / 133 . | 51.41 | 0.84 | 3.72 | 1.02 | 4.92 | 0.12 | 16.48 | 21.03 | 0.38 |
| 1 / 134 . | 51.72 | 1 | 3.87 | 0.83 | 4.84 | 0.06 | 16.42 | 21.34 | 0.38 |
| 1 / 135 . | 51.1 | 1.14 | 4.42 | 0.83 | 5.04 | 0.12 | 16.09 | 21.41 | 0.39 |
| 1 / 136 . | 51.35 | 1.05 | 4.65 | 0.82 | 4.88 | 0.1 | 16.24 | 21.14 | 0.38 |
| 1 / 137 . | 51.6 | 0.89 | 4.21 | 0.97 | 4.93 | 0.08 | 16.29 | 21.22 | 0.39 |
| 1 / 138 . | 51.5 | 0.84 | 4.08 | 1.08 | 4.9 | 0.11 | 16.31 | 21.01 | 0.39 |
| 1 / 139 . | 51.67 | 0.92 | 4.08 | 1 | 4.88 | 0.09 | 16.54 | 21.33 | 0.39 |
| 1 / 140 . | 51.65 | 0.99 | 4.01 | 0.8 | 4.89 | 0.1 | 16.65 | 21.29 | 0.39 |
| 1 / 141 . | 51.88 | 0.85 | 4.14 | 0.96 | 4.81 | 0.13 | 16.47 | 21.28 | 0.39 |
| 1 / 142 . | 51.71 | 0.85 | 4.14 | 1.05 | 4.83 | 0.13 | 16.54 | 21.08 | 0.4 |
| 1 / 143 . | 51.52 | 0.89 | 4.18 | 1.15 | 4.75 | 0.1 | 16.41 | 21.25 | 0.4 |
| 1 / 144 . | 51.66 | 0.81 | 4.08 | 1.07 | 4.77 | 0.13 | 16.36 | 21.35 | 0.4 |
| 1 / 145 . | 51.52 | 0.83 | 3.99 | 1.08 | 4.51 | 0.1 | 16.42 | 21.32 | 0.39 |
| 1 / 146 . | 51.37 | 0.86 | 3.98 | 1.1 | 4.61 | 0.07 | 16.23 | 21.53 | 0.39 |
| 1 / 147 . | 50.07 | 0.88 | 3.87 | 1.04 | 4.53 | 0.12 | 16.23 | 20.85 | 0.37 |
| 1 / 148 . | 50.65 | 1 | 4.21 | 0.95 | 4.7 | 0.11 | 16.2 | 21.31 | 0.39 |
| 1 / 149 . | 50.58 | 0.82 | 4.02 | 0.97 | 4.59 | 0.06 | 16.37 | 21.26 | 0.39 |
| 1 / 150 . | 50.94 | 0.81 | 3.8 | 0.93 | 4.58 | 0.09 | 16.39 | 21.32 | 0.38 |